

Key Points:

- Many different surface processes are actively shaping the geomorphology of Mars today
- Current surface changes must be understood in order to correctly interpret changing environments over time
- Several active Martian processes were not predicted and lack a terrestrial analog

Correspondence to:

C. M. Dundas,
cdundas@usgs.gov












Citation:

Dundas, C. M., Becerra, P., Byrne, S., Chojnacki, M., Daubar, I. J., Diniega, S., et al. (2021). Active Mars: A dynamic world. *Journal of Geophysical Research: Planets*, 126, e2021JE006876. <https://doi.org/10.1029/2021JE006876>

Received 24 FEB 2021
Accepted 21 JUN 2021

© 2021. The Authors. This article has been contributed to by US Government employees and their work is in the public domain in the USA. This is an open access article under the terms of the [Creative Commons Attribution-NonCommercial-NoDerivs License](#), which permits use and distribution in any medium, provided the original work is properly cited, the use is non-commercial and no modifications or adaptations are made.

Active Mars: A Dynamic World

Colin M. Dundas¹ , Patricio Becerra² , Shane Byrne³ , Matthew Chojnacki⁴ , Ingrid J. Daubar⁵ , Serina Diniega⁶ , Candice J. Hansen⁴ , Kenneth E. Herkenhoff¹ , Margaret E. Landis⁷ , Alfred S. McEwen³, Ganna Portyankina⁷ , and Adomas Valantinas² 

¹U.S. Geological Survey, Astrogeology Science Center, Flagstaff, AZ, USA, ²Physikalisches Institut, Universität Bern, Bern, Switzerland, ³Lunar and Planetary Laboratory, University of Arizona, Tucson, AZ, USA, ⁴Planetary Science Institute, Tucson, AZ, USA, ⁵Department of Earth, Environmental, and Planetary Sciences, Brown University, Providence, RI, USA, ⁶Jet Propulsion Laboratory/California Institute of Technology, Pasadena, CA, USA, ⁷Laboratory for Atmospheric and Space Physics, University of Colorado, Boulder, CO, USA

Abstract Mars exhibits diverse surface changes at all latitudes and all seasons. Active processes include impact cratering, aeolian sand and dust transport, a variety of slope processes, changes in polar ices, and diverse effects of seasonal CO₂ frost. The extent of surface change has been surprising and indicates that the present climate is capable of reshaping the surface. Activity has important implications for the Amazonian history of Mars: understanding processes is a necessary step before we can understand their implications and variations over time.

Plain Language Summary Many surface processes are active across the surface of Mars, producing changes that can be observed from orbit and by landed missions. The observed changes include new impact craters, sand and dust transported by the wind, a variety of flows on slopes, and many changes to perennial ice deposits. Many changes are driven by seasonal CO₂ frost. These changes indicate that surface evolution on Mars is ongoing and not confined to past climate conditions.

1. Introduction

An axiom of geology is that the present is the key to the past. Knowledge of current processes and their consequences is an essential tool for understanding history, including the ancient rock record and the associated climate. Modern Mars is cold, with a thin atmosphere, and has previously been thought to have little ongoing geomorphic activity—especially when compared with ancient Mars, which had apparent large-scale, Earth-like processes, as inferred from ancient landforms. This interpretation has led much research to focus not on the present Martian environment, but rather on Mars' early conditions and climate change over time. However, in recent years, observations of ongoing surface changes have proliferated, demonstrating that Mars' landscape is actively evolving and likely has been throughout the Amazonian epoch. These observed geomorphic changes shed light on a variety of active processes, some with no terrestrial analog, and reveal present-day Mars to be a dynamic world. This in turn may mean that more of the ancient and recent Martian geologic record can be explained without dramatic climate change.

This work presents a comprehensive summary and categorization of the many types of observed changes on the Martian surface. Aeolian and frost-related surface activity are discussed in more detail in a parallel review by Diniega et al. (2021), which focuses on connecting specific landforms to their formative processes; the focus herein is to provide a broad overview of known types of changes in surface morphology and albedo. Weather and seasonal frost and ice are not discussed in detail here, except where necessary to describe their effects on the surface; observations of the atmosphere were reviewed by M. D. Smith (2008) and Martínez et al. (2017), and seasonal frost is discussed in Piqueux, Kleinböhl, et al. (2015) and references therein. Weathering and other microscale or chemical processes are not discussed. Even with these exclusions, the scope of the subject is broad and we have focused on the key discoveries and constraints.

Studying surface changes on Mars yields a unique look at processes within an un-Earthly environment. Annual-mean surface temperatures range from ~160 K at the poles to ~230 K at the equator, with extreme diurnal ranges compared with the Earth (e.g., Kieffer, 2013). Atmospheric pressure varies from >1,000 Pa in the Hellas basin to <100 Pa at the summit of Olympus Mons. In the winter, temperatures at mid- and

Table 1
Medium and High Resolution Orbital Imagers

Spacecraft	Imager	Characteristics	Reference
Mars Global Surveyor (MGS)	Narrow Angle Mars Orbiter Camera (MOC-NA)	1.5 m/pix	Malin et al. (1992, 2010)
Mars Reconnaissance Orbiter (MRO)	Context Camera (CTX)	6 m/pix	Malin et al. (2007)
Mars Reconnaissance Orbiter (MRO)	High Resolution Imaging Science Experiment (HiRISE)	0.25 m/pix; three-color central swath	McEwen et al. (2007)
ExoMars Trace Gas Orbiter (TGO)	Colour and Stereo Surface Imaging System (CaSSIS)	4.6 m/pixel; four colors	N. Thomas et al. (2017)

high-latitudes drop to the condensation point of CO₂, resulting in seasonal dry ice frost caps more than a meter thick in the polar regions. Surface pressure varies seasonally by ~30%, as formation of this ephemeral frost removes a significant fraction of the atmosphere (e.g., Leighton & Murray, 1966; M. D. Smith, 2008). This seasonal CO₂ frost extends to around 50° latitude in each hemisphere (e.g., Piqueux, Kleinböhl, et al., 2015), or lower latitudes on pole-facing slopes. Thin diurnal H₂O and CO₂ frosts are widespread and can even occur at equatorial latitudes (e.g., Martínez et al., 2016; Piqueux et al., 2016).

Studies of active surface processes have been enabled by the continuous presence of active spacecraft in Mars orbit for more than two decades. While many different instruments have contributed to understanding Mars' modern surface, the most important for identifying and monitoring active processes have been medium- and high-resolution imagers (Table 1) capable of repeat imaging of the same locations, enabling the detection of changes in albedo and topography. These instruments have revealed surface changes in exquisite detail.

Mars has strong seasonal variations and year-to-year differences in atmospheric conditions, so it is necessary to use a Martian calendar for discussion of active processes rather than referring to dates on Earth. The Mars calendar now in wide use (Clancy et al., 2000; Piqueux, Byrne, et al., 2015) has Mars Year (MY) 1 beginning at $L_S = 0^\circ$ on April 11, 1955, and it is MY 36 at the time of writing. Seasons on Mars are given by L_S , the areocentric longitude of the Sun. Northern spring begins at $L_S = 0^\circ$ and northern autumn at $L_S = 180^\circ$. Because perihelion (the closest approach to the Sun) currently occurs at $L_S = 251^\circ$, southern hemisphere seasons are more extreme, with a longer winter and shorter, warmer summer; however, the season of perihelion varies over the whole Martian year with a period of 51 kyr, which is short compared to the time the climate has been in its cold, dry state.

2. Impact Cratering

New impact craters (Figure 1) were first confirmed (Malin et al., 2006) with the Mars Orbiter Camera (MOC) onboard the Mars Global Surveyor (Malin et al., 1992, 2001). Continued surveys using the combination of the Context Camera (CTX; Malin et al., 2007) and High Resolution Imaging Science Experiment (HiRISE; McEwen et al., 2007) on the Mars Reconnaissance Orbiter have greatly expanded this data set (Daubar et al., 2013, 2020) so that more than a thousand new impact sites are known, with crater diameters ranging from below HiRISE resolution up to tens of meters. Malin et al. (2006) reported one substantially larger (148 m) candidate new crater but it is now considered unlikely to be new, based on higher-resolution observations that show bedforms on the floor (Bridges et al., 2007); the inclusion (or not) of this crater in the set of newly formed craters has implications for the formation rate of craters of this size (Aharonson, 2007). These observations provide direct measurements of the present-day impact rate and give constraints on the crater size-frequency production function in recent time. The impact flux estimated from these observations is 1.65×10^{-6} impacts (with effective crater diameter ≥ 3.9 m) per km² per Earth year (Daubar et al., 2013). "Effective diameter" reflects the observation that approximately half of the new impacts form clusters due to fragmentation in the atmosphere, sometimes with many constituent craters. The clusters are reconstituted into an estimated equivalent single impact defined as the cube root of the sum of the cubes of the individual crater diameters for inclusion in a production function. The occurrence of fragmentation and crater clusters rather than single craters may be dependent on atmospheric pressure (Daubar et al., 2019).

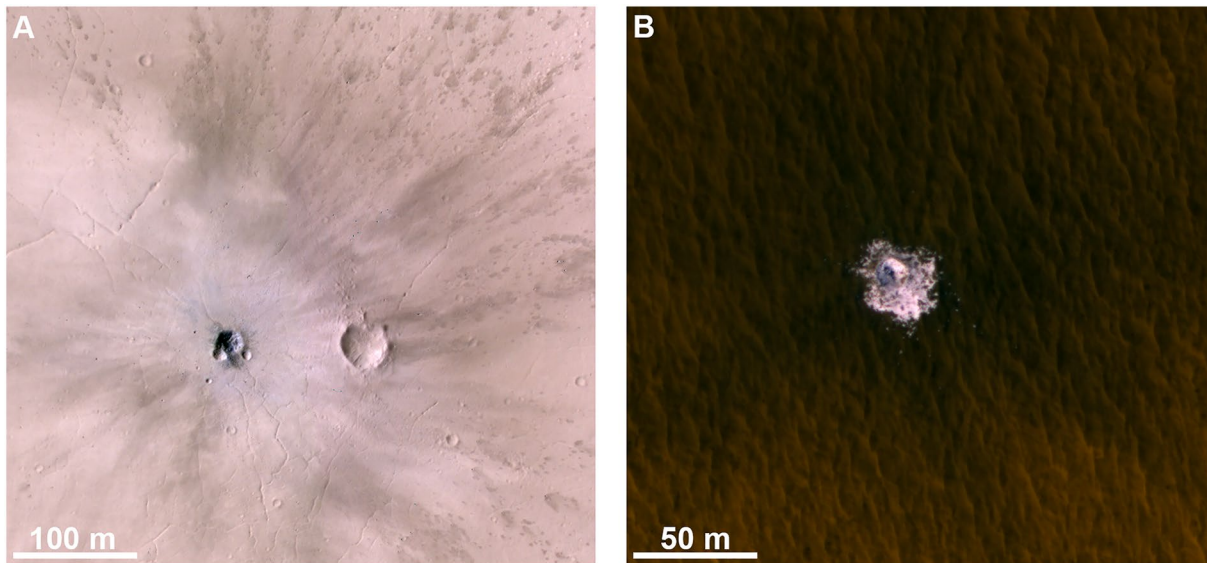


Figure 1. Examples of new impact craters, including well-defined blast pattern (a) and ice exposure (b) ((a): Subsection of High Resolution Imaging Science Experiment [HiRISE] image ESP_045270_1950. (b): Subsection of HiRISE image ESP_025840_2240. North is up and illumination from the left. All image figures have been stretched to optimize contrast and visibility; original data are available as described in the Data Availability statement).

The impact rate is important because craters are a major component of Martian geomorphology, and because impact craters represent an important tool for relative age-dating of planetary surfaces, yielding an absolute surface exposure age when properly calibrated. Daubar et al. (2013) suggested that there is as much as an order-of-magnitude deficit between the observed impact flux and previous theoretical predictions. This may be due to the contribution of background secondary craters in the predicted long-term flux (Hartmann & Daubar, 2017). However, the shallower slope of the Daubar et al. (2013) production function, if extrapolated, would imply that primary craters with diameter >50 m are produced more rapidly than the theoretically estimated combined flux of primary and secondary impacts. This could be resolved if the primary production function slope increases at larger diameters, or if the slope at small diameters has been underestimated due to incomplete detection of smaller craters. New craters on the Moon have a much steeper size-frequency distribution (power law exponent of -4.64 ± 0.50 ; Speyerer et al., 2016) than observed for Mars (-2.45 ± 0.36 ; Daubar et al., 2013), which is inconsistent with Martian results if new, small impacts are dominated by asteroids for both worlds and if the data sets do not have systematic biases affecting their slope not accounted for by the formal errors. However, such biases are possible for Mars due to the target-dependent detection of new craters; a much larger data set is now available and may provide new insights in the future (Daubar et al., 2020).

Large seasonal variations in the impact rate through the year as a function of solar distance have been predicted, with as many as $20\times$ more potential impactors at aphelion than perihelion (Ivanov, 2001), although more recent models by JeongAhn and Malhotra (2015) indicate that there should be a lower aphelion-to-perihelion impact flux ratio of ~ 3 . The data do not show a large variation, but interpretation is complicated by potential biases in the temporal collection of data and loose timing constraints on events (Daubar et al., 2012).

Because the areal coverage by the highest-resolution imagers (MOC-Narrow Angle and HiRISE) is limited to a few percent of the surface with very limited areas of repeat imaging, the vast majority of new impact sites have been detected in CTX images (Daubar et al., 2013). This is possible because impact events make relatively large disturbances in surface dust that can be $>100\times$ larger than the crater (Bart et al., 2019) and therefore are detectable in medium-resolution images. Detections are thus biased toward dusty, high-albedo regions. This bias could affect the production function derived from the impacts, due to target effects on crater properties (dust is weaker and more porous than regolith), or size- or region-dependence of detections affecting the completeness of detections. The size of the dark halo is a function of the impact energy but also depends on surface properties and local atmospheric pressure (Bart et al., 2019). The vertical scale of

the effect of the halos is not well constrained; however, Bart et al. (2019) found that for the smallest craters (<8 m diameter) the halo size is slightly dependent on thermal inertia but not dependent on a dust cover index. Because the former is controlled by the surface properties at depths of centimeters while the latter is only sensitive to tens of microns, the vertical scale of the effects of halos likely falls somewhere between those two thicknesses.

Impact blast zones fade over time. At tropical latitudes, this fading typically occurs over several decades (Daubar et al., 2016). High-latitude features within the zone covered by seasonal CO₂ ice caps (above ~50° N/S latitude) typically disappear during the first winter after impact (Dundas et al., 2014), due either to deposition of dust incorporated in the frost the cap or sublimation at the base of the CO₂ (discussed in Section 5.1).

New craters also have a surprising application in studies of subsurface H₂O ice, as impacts at mid- and high-latitudes commonly expose shallow ice (Byrne et al., 2009; Dundas et al., 2014). H₂O ice has been observed in craters (Figure 1b) at latitudes as low as 39°N, which has implications for the recent climate: the stability of ice may require a long-term average atmospheric water content somewhat higher than at present (Dundas et al., 2014), although that value could date to the time of deposition of the ice. The ice remains distinct from regolith in color for months or years, indicating that it has a low lithic content, but it slowly fades to match the background surface (Dundas & Byrne, 2010; Dundas et al., 2014). This may be due to both ice sublimation and dust deposition from the atmosphere or the seasonal cap, but the former is likely more important since blast zones can remain distinct for longer than the icy coloration persists. Shrinking and disappearance of ice-rich ejecta blocks have also been observed (Dundas et al., 2014).

3. Aeolian Changes

3.1. Albedo Changes

Here, we primarily discuss changes to the frost-free surface; deposition and removal of frost create dramatic temporary changes to the albedo, but we focus on changes to the underlying surface. Albedo changes on Mars were observed telescopically in the pre-spacecraft era (see Martin et al., 1992 for a summary). Prior to spacecraft exploration, some investigators attributed these variations in brightness and color to vegetation changes, but others correctly inferred that they were due to aeolian processes. Regional-scale albedo changes over years to decades have been documented by more recent orbital instruments (e.g., Geessler, 2005; Geessler et al., 2016; Sagan et al., 1973) and have been attributed to seasonal dust transport by storms, high winds, and dust devils. Albedo changes can be produced through the addition or removal of very small amounts of surface dust, and thus in most cases likely represent movement of a very thin veneer. A dust layer thickness of tens of microns can be completely opaque, obscuring the color of the underlying material, while a coating just 1–2 microns thick is sufficient to markedly alter the reflectance (Fischer & Pieters, 1993; Wells et al., 1984). Observations by the *Spirit* rover combined with orbital imaging support the idea that thin dust coatings have a strong effect on albedo, as surface darkening was associated with removal of fine dust from larger sand grains while the sand grains moved short distances of <0.7 mm (Greeley et al., 2005).

Wind streaks many kilometers in scale are one component of regional albedo changes seen in early orbiter data (e.g., Sagan et al., 1972, 1973; Veverka et al., 1977). Different types of wind streaks were described by P. C. Thomas et al. (1981). They found that bright streaks, attributed to preferential dust deposition, showed minor variability. In contrast, dark erosional streaks changed significantly due to deposition and removal of traces of dust. Large dust storms deposited dust, which erased the dark erosional streaks entirely, but new streaks formed within weeks after the atmosphere cleared. Dark depositional streaks also exist. P. C. Thomas et al. (1981) termed these “splotch-related streaks” as they emanate downwind from dunes and sand bodies, and some were observed to change intermittently. Smaller, sub-kilometer bright or dark streaks associated with craters or topographic knobs are more variable in orientation than larger streaks (Day & Dorn, 2019; Day & Rebolledo, 2019; Fenton et al., 2015). Geessler et al. (2008) investigated an active dark wind streak on the rim of Victoria crater. They found that the streak was dark due to reduced surface dust and, based on *Opportunity* observations of active sand transport in the streak, favored an origin by deposition of sand within it. However, this particular wind streak may not be representative of all dark streaks that form in the lee of obstacles. Instead, the streak at Victoria crater resembles the “splotch-related streaks” of

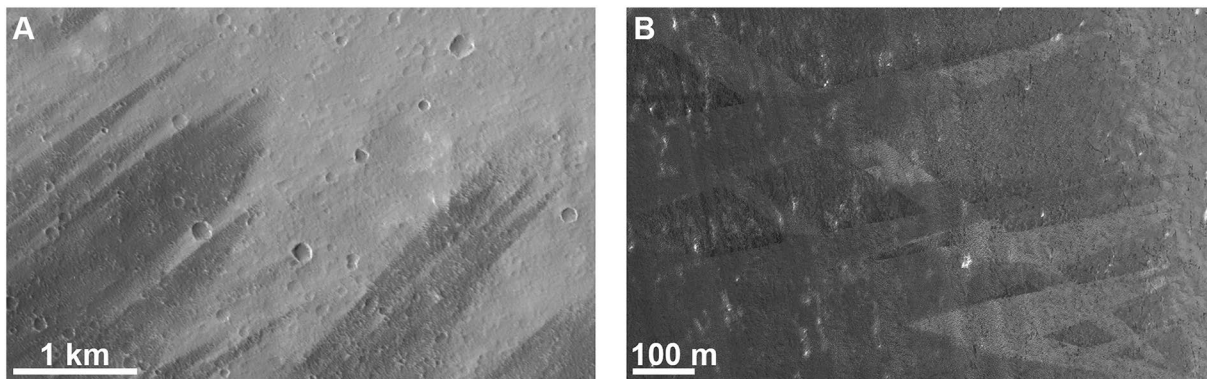


Figure 2. (a) Spire streaks on Pavonis Mons. (b) Complex streak superposition on the North Polar Layered Deposits ((a): Subsection of Context Camera image P02_001893_1804_XN_00N113W. North is up and illumination from the left. (b): Subsection of High Resolution Imaging Science Experiment image PSP_009273_2610. North is to the upper right and illumination from lower left).

P. C. Thomas et al. (1981). Toyota et al. (2011) reported changes in spindle-shaped “spire streaks” on several large volcanoes in Tharsis. These streaks (Figure 2a) are darker than their surroundings and have point sources, often without any topographic feature at the source. The streaks indicate dust removal, potentially due to saltation clouds that widen as they progress downwind (Toyota et al., 2011) but likely do not remove the entire dust layer. The edges may be sharp at CTX scale (6 m/pix) but ragged and serrated at HiRISE scale (25 cm/pix) (Dundas, 2020b). Wind streaks may also form in the wake of large craters as collections of large ripples, whereas adjacent areas lack bedforms (Silvestro et al., 2015).

Dust transport has also been observed at the surface. Viking Lander 1 made early in situ observations of aeolian particle transport. Erosion and deposition of tens to hundreds of microns of fine-grained red dust occurred on several occasions (Arvidson et al., 1983). Arvidson et al. (1983) and Moore (1985) also reported changes associated with a major storm system and high winds. Most of the changes were associated with materials disturbed by the lander, such as erosion of dump piles, indicating that the undisturbed surface (other than the coating of dust) was sufficiently cohesive and equilibrated to be minimally affected by the winds (Arvidson et al., 1983; Moore, 1985). Dust deposition and removal were observed by both the *Spirit* and *Opportunity* rovers (Greeley et al., 2005; Sullivan et al., 2005, 2008). Although both rovers were at near-equatorial latitudes, the observed dust transport displayed different annual cycles (Kinch et al., 2015). *Spirit* observed dust deposition from late southern summer to late southern winter, followed by removal. *Opportunity* observed a semi-annual cycle with two deposition/erosion cycles, switching from deposition to removal around $L_s = 45^\circ$ and 225° . Dust-clearing events for the *Opportunity* rover solar panels occurred near the beginning of dust devil season during three Mars years (Lorenz & Reiss, 2015).

Actively changing wind streaks are also observed in the polar regions (Figure 2b), where they are apparently formed by mobilized water-ice grains (Herkenhoff et al., 2020). Bright and dark streaks have been observed at the periphery of the north polar residual cap by previous Mars orbiters and were the target of repeat HiRISE observations. The complex interactions between overlapping bright and dark streaks in some of these HiRISE images (Figure 2b) indicate that formation of the streaks involves processes more complex than simply the emplacement of dark veneers (cf. Rodriguez et al., 2007). Bright and dark streaks are seen to evolve during the northern summer, which is evidence for active aeolian redistribution of water frost and perhaps darker (nonvolatile) dust or sand. HiRISE color images taken during MY 29 do not include the area shown in Figure 2b, but part of this area was imaged in color during MY 30. This and other color images of similar streaks show that the red:blue ratio of the bright streaks is consistent with partial frost cover. While the color and albedo of the streaks are observed to change during the summer season and interannually, the surface texture does not, suggesting that mobility of dark, nonvolatile material has a negligible effect on the underlying topography. The sharp boundaries of the streaks are similar to those seen along spire streaks in dust (Toyota et al., 2011), perhaps formed by advancing clouds of saltating particles.

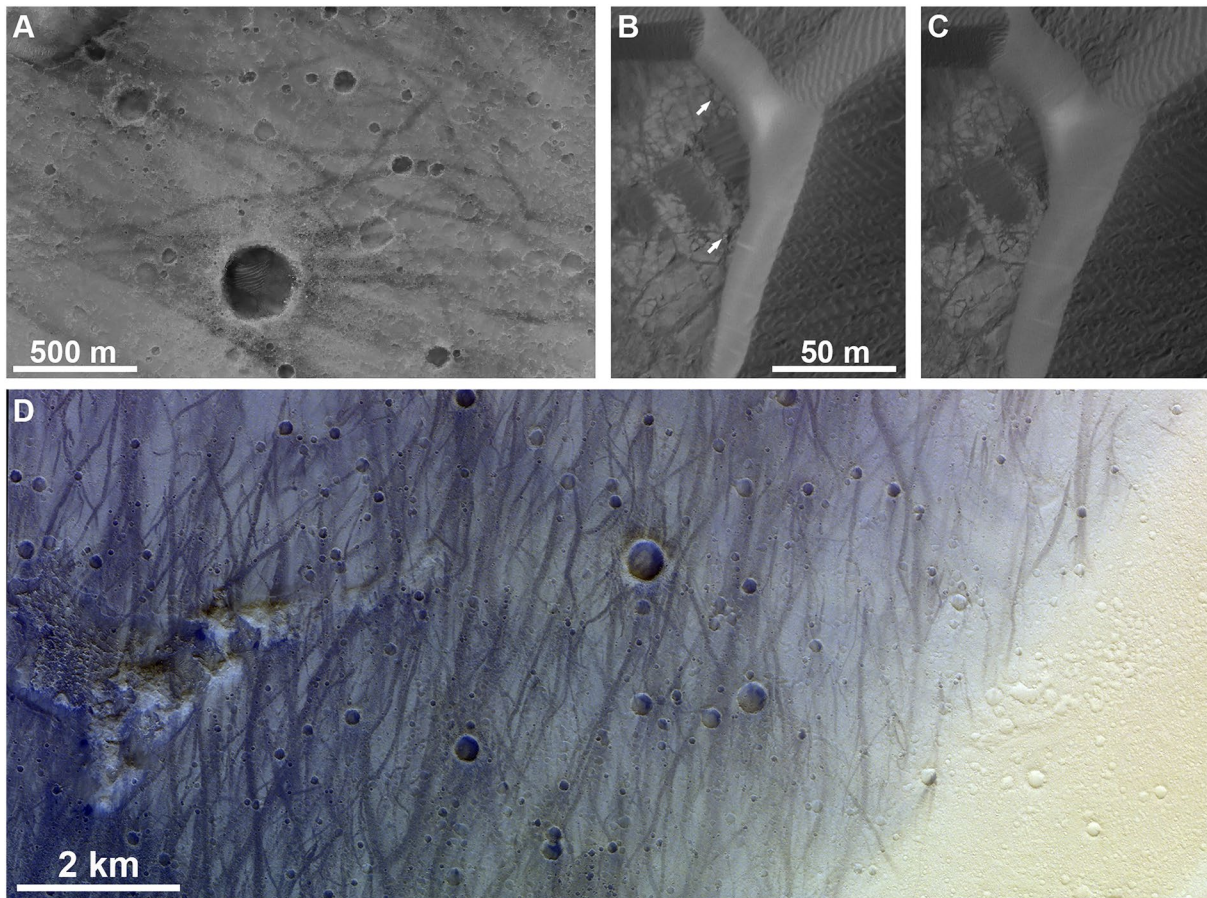


Figure 3. Active aeolian features on Mars. (a) Dust devil tracks in Gusev crater. (b and c) Advancing dune and changing ripples in Nili Patera. Note bedrock features indicated by arrows which are buried by sand in (c). (d) Dust devil tracks in Gusev crater confined to a region of thin dust cover ((a): Subsection of High Resolution Imaging Science Experiment [HiRISE] image PSP_005456_1650. (b): Subsection of HiRISE image ESP_017762_1890 [Mars Year, MY 30, $L_S = 89^\circ$]. (c): Subsection of HiRISE image ESP_062069_1890 [MY 35, $L_S = 97^\circ$]. (d): Colour and Stereo Surface Imaging System color image MY34_003860_344_1 [NIR, PAN, BLU filters]. North is up and illumination is from the left in (a–c). In (d), north is to the right and illumination is from the bottom right. In all comparison pairs such as (b and c), the panels are shown at the same resolution).

3.2. Dust Devil Tracks

Dust devil tracks (Figure 3a) are one of the most widespread indicators of aeolian surface change on Mars. Current studies of dust devils and their tracks were comprehensively summarized in a recent special issue (Reiss, Lorenz, et al., 2016, and references therein). The tracks are generally thought to result from removal of a thin dust coating on a darker substrate, although some are brighter than their surroundings (Reiss et al., 2011). In some cases, the tracks may not have formed through complete dust removal; instead, the removal of only some surface dust exposes larger-grained materials that change the photometric properties, resulting in lower-albedo tracks (Reiss, Fenton, et al., 2016). The brightness of Martian soils can also be affected by roughness, porosity, and compaction (e.g., Herkenhoff et al., 2004) so a grain size difference may not be required. The tracks are usually darker than their surroundings, tens of meters wide and kilometers long, and change in appearance over short timescales (Daubar et al., 2018; Malin & Edgett, 2001; Verba et al., 2010). Cantor et al. (2006) provide a thorough summary of MOC and earlier orbital observations of dust devils and their tracks. Dust devils and track formation are most common in summer in each hemisphere but can occur in other seasons (Cantor et al., 2006; Whelley & Greeley, 2008), and large dust devils are concentrated in particular regions. The tracks are found at almost all latitudes except over polar ice, and at all elevations including the summit of Arsia Mons at more than 16 km elevation (Cushing et al., 2005). However, only ~14% of dust devils visible to MOC produce tracks (Cantor et al., 2006).

Cantor et al. (2006) also found that dust devils lift enough dust (estimated global flux of $4 \times 10^{-3} \text{ kg m}^{-2} \text{ MY}^{-1}$, when correcting for the estimated fraction of dust devils observed by MOC) to be major contributors to the background dust opacity of the atmosphere. However, others have shown that dust devils are not the major drivers of changes in global dust cover (Geissler et al., 2016; Szwast et al., 2006). Whelley and Greeley (2008) estimated a total dust lifting of $(1.6 \pm 0.7) \times 10^{-3} \text{ kg m}^{-2} \text{ MY}^{-1}$, concentrated between $45\text{--}75^\circ$ latitude in each hemisphere. This is approximately half the estimate by Cantor and coworkers, though in fair agreement as there are many assumptions that may not be reflected in the formal uncertainties. Ground-based studies by the *Spirit* rover complement orbital observations (Greeley et al., 2006, 2010) and provide detail that cannot be seen in those temporally sparse, lower-resolution observations. Dust devils are an important influence on the surface of Gusev crater, lofting a minimum average of $\sim 18 \times 10^6 \text{ kg}$ of dust from an area of $\sim 3,000 \text{ km}^2$ each Mars year. This corresponds to stripping an average of a few microns of dust across the region, which would be only a thin veneer, though one sufficient to strongly affect surface albedo. Verba et al. (2010) estimated that fewer than 1% of dust devils observed by the rover left tracks visible from orbit. This estimate likely differs from the Cantor et al. (2006) value because many more small dust devils can be observed from the surface, and the smaller vortices are less likely to be strong enough to completely remove the surface dust coating. However, an additional factor may be that faster-moving dust devils do not remove as much dust at any given point (Lorenz & Reiss, 2015). The InSight lander has detected numerous convective vortices (i.e., the atmospheric phenomenon that creates a dust devil if dust is lofted) and, over the same time period, the Mars Reconnaissance Orbiter has documented the formation of dust devil tracks at that location. However, no active dust devils have yet been detected in either orbital or surface images (Banfield et al., 2020; Perrin et al., 2020) in this time period. Dust devils were also initially thought to be rare at the *Curiosity* landing site, but were subsequently found to be common although faint (Lemmon et al., 2017).

Multiple observations of individual dust devils have enabled estimates of wind velocities, including both the translation rate of the dust devil and the tangential velocity associated with rotation. Cantor et al. (2006) inferred a tangential wind velocity of $26\text{--}50 \text{ m s}^{-1}$ for one example in Viking images, and Choi and Dundas (2011) reported tangential velocities exceeding 30 m s^{-1} in a sample of four more vortices, with translational velocities sometimes exceeding 20 m s^{-1} . Stanzel et al. (2008) measured translational velocities of $1\text{--}59 \text{ m s}^{-1}$ for a large sample of dust devils observed from orbit, and Reiss et al. (2014) reported speeds of $4\text{--}25 \text{ m s}^{-1}$. Greeley et al. (2010) reported horizontal (translational) speeds up to 27 m s^{-1} and vertical speeds up to 10 m s^{-1} in Gusev crater, but the median values were substantially lower ($1.5\text{--}2.5$ and $1.0\text{--}1.6 \text{ m s}^{-1}$, respectively). Orbital detections are likely biased toward the largest, strongest vortices: the dust devil in Gusev crater analyzed by Choi and Dundas (2011) showed velocities $>30 \text{ m s}^{-1}$, greater than any of the surface detections.

3.3. Bedform Movement

While dust-lifting effects have been observed for decades, direct confirmation of active sand transport by the wind (Figures 3b and 3c) is more recent. Sand dunes were observed in the earliest spacecraft images, but no changes were identified in dune crests or margins until very recently (summarized in Diniega et al., 2017 and references therein). Edgett and Malin (2000) reported dark streaks superposed on frosted dunes, as well as slipface striations interpreted as evidence for sand avalanches. The slipface striations provided evidence for sand movement and, given the sharp dune crestlines, suggested that wind-driven sand transport was creating the steepened lee slopes. Fenton (2006) documented changing slipface streaks in Rabe crater, which were used to infer that the dunes were active with a migration rate of $1\text{--}2 \text{ cm/MY}$, although CO_2 frost-related processes may also have modified dune slopes during that period. More recently, definitive evidence for bedform migration in orbital images has emerged, thanks to longer temporal baselines and higher image resolution. Bourke et al. (2008) reported the shrinking and disappearance of decameters-scale dome dunes in the north polar erg, indicating erosion of hundreds of cubic meters of sand over several Mars years. Silvestro et al. (2010) documented decimeter-scale ripples in Nili Patera that migrated 1.7 m over 4 months. These HiRISE-based observations of active ripples overturned earlier notions that these grooved textures were indicative of sand induration and erosion (Edgett & Malin, 2000). After Chojnacki et al. (2011) reported erosion and migration of dome dunes in Endeavor crater, detections of ripple and dune movement have subsequently proliferated planet-wide (Banks et al., 2018; Bridges, Bourke, et al., 2012; Bridges et al., 2013; Chojnacki et al., 2015, 2019; Hansen et al., 2011; Runyon et al., 2017).

Ayoub et al. (2014) demonstrated seasonal variations in sand flux in Nili Patera, with maximal activity correlating with peak atmospheric pressure in southern summer. Similar seasonality was also observed at nearby Meroe Patera, while Gale crater had a less defined seasonal signal (Roback et al., 2019). Chojnacki et al. (2017) showed factor-of-five year-to-year variations at some dunes in Meridiani Planum. Sand fluxes of $1\text{--}20\text{ m}^3\text{ m}^{-1}\text{ yr}^{-1}$ are common on Mars, with values up to $35\text{ m}^3\text{ m}^{-1}\text{ yr}^{-1}$ observed (Bridges, Ayoub, et al., 2012; Chojnacki et al., 2019), which were derived based on dune migration rates and heights. These values are comparable to slow-moving, low-flux sand dunes on Earth. These are bulk values for the dune sand flux, which are around $5\times$ higher than the contribution from ripple migration alone (Bridges, Ayoub, et al., 2012). The sand flux varies strongly, with high sand transport rates observed in Syrtis Major, the Hellespontus Montes, and the north polar erg (Chojnacki et al., 2019).

Although there are now numerous observations of movement of dark dunes and ripples, large bedforms referred to as Transverse Aeolian Ridges (TARs) initially did not show detectable activity (Bridges, Bourque, et al., 2012; Bridges et al., 2013), and it was suggested that they were last active under different climate conditions several million years ago (Balme et al., 2008; Berman et al., 2011; Geissler, 2014). However, Silvestro et al. (2020) recently reported movement of some brighter bedforms described as megaripples or small TARs, although with inferred sand fluxes two orders of magnitude lower than that estimated for adjacent migrating dunes. Continued observation of TARs and megaripples in other areas of Mars would be needed to confirm whether these bedforms (or at least specific examples of them) are active in the present Mars climate (Chojnacki et al., 2020; Zimbelman, 2019).

When interpreting these features and observed activity, it is also important to recognize that classification of Martian aeolian bedforms is challenging, especially as many of these features may be named based on geomorphic similarities to certain terrestrial features or to other Martian features. However, neither bright TARs (10–100 m spacing/wavelength, 1–14 m tall) nor the large dark ripples (1–5 m spacing, ~ 40 cm tall) observable from orbit closely correspond to widely reported terrestrial analogs (Balme et al., 2008; Lapotre et al., 2016), and the former may be polygenetic as some have been interpreted as dust bedforms (Geissler, 2014). Although TAR-like features are not common on Earth, new observations of moderate-scale aeolian bedforms (2–250 m wavelength, 1–4 m tall) were identified in the deserts of Iran and Libya (Foroutan & Zimbelman, 2016; Foroutan et al., 2019) and provide a terrestrial analog. Large, dark ripples on Mars show asymmetric topographic profiles at scales that differ from any known aeolian bedform on Earth, and may be more analogous to subaqueous “drag” ripples, which can form transiently on Earth (Lapotre et al., 2016, 2018). Alternatively, a saltation impact splash mechanism is argued to be efficient in the low dynamic pressure of Mars and permit a wider range of ripple sizes (Sullivan & Kok, 2017; Sullivan et al., 2020). In light of this complexity, and with detections of movement growing as observational baselines extend, it may be premature to draw any strong conclusions about whether any bedforms are completely inactive at present, other than bedforms that preserve impact craters and thus are likely indurated (e.g., Chojnacki et al., 2020; Edgett & Malin, 2000; Golombek et al., 2010).

Sand transport has also been observed from the surface. Moore (1985) reported the appearance of small bedforms (4–5 cm wavelength) in the Sol 1740 wind event at Viking Lander 1 (“Sol” refers to the Martian day of the mission since landing). He could not determine whether they were newly formed or simply exhumed, but subsequent observations have demonstrated mobility of similarly sized bedforms elsewhere on Mars, so formation appears likely. Sullivan et al. (2008) reported migration of small ripples in Gusev crater during the MY 28 global dust storm, with a displacement of 2 cm over five sols. Geissler et al. (2010) documented changes in tracks left by the rovers *Spirit* and *Opportunity*, finding that they were primarily erased by saltating sand, rather than atmospheric dust fallout. Most recently, the *Curiosity* rover has studied ripples and dunes in the “Bagnold” dune field in Gale crater. Bridges et al. (2017) reported negligible dune and large ripple activity in the aphelion season (northern spring and summer) when wind speed and atmospheric density are low, but Baker et al. (2018) observed small ripple migration of up to 2.8 cm/sol during the perihelion season, similar in seasonality to the Nili Patera large ripple observations of Ayoub et al. (2014). Those migrating ripples were small-scale features analogous to terrestrial wind ripples rather than the intermediate-scale ripple bedforms observable from orbit.

Early studies that extrapolated Earth-based models of aeolian sand transport to the Martian environment estimated that sand saltation under present-day Martian conditions would require winds speeds of 50–

Table 2
Categories of Low/Midlatitude Slope Processes on Mars

Category	Setting	Relative brightness	Typical morphology	Timing
Gully flows	Gully landforms, mid/high latitude	Brighter, darker, neutral; may be distinct in color	Point source, widens downslope; 100–1,000 m	Local winter; single event
RSL	Low-albedo angle-of-repose slopes	Darker when active	Near-constant width < 5 m, closely follows downhill gradient	Typically forms gradually at warmest time and fades when inactive; RSL fade and recur annually but morphologically similar slope lineae may persist for multiple years or fade incompletely
Slope lineae	Recommended generic term for features that morphologically resemble RSL but do not match temporal behavior			
Slumps	Valles Marineris, downslope from RSL	Darker	Arcuate headscarp and lobate terminus	$L_S = 0\text{--}120^\circ$; single event
Dune alcoves	Sand dunes, primarily N. polar erg	Neutral	Alcove feeding apron on slipface; tens of meters	Initial event after early frost, enhanced by spring activity?
Slope streaks	Dusty (high-albedo) steep slopes	Darker when new	Point source; 10–1,000 m, often do not follow steepest downhill gradient	Year-round, but concentrated in autumn; single event
Blockfalls	Steep slopes	Brighter or darker	Discontinuous bounce marks	X (presumed single event)
Rock shifts	High-latitude slopes	N/A	Boulder translated < 10 m	X

Note. See main text for references. Characteristics are for typical features, not the complete range of morphologies. X indicates that a parameter is not well described or well constrained in the current literature.

Abbreviation: RSL, recurring slope lineae.

135 m/s (e.g., Greeley et al., 1976), and Moore (1985) suggested that the erosion observed by Viking Lander 1 required winds of 40–50 m/s at the height of the meteorology boom (located 1.6 m above ground level). Such speeds are rarely attained, yet both sand and dust are clearly mobile. For sand, the solution appears to be the wide separation of the impact and fluid thresholds for saltation under Martian conditions (Kok, 2010), permitting extensive sand transport to be triggered once a relatively small number of particularly susceptible grains are set in motion (Sullivan & Kok, 2017). This allows a more vigorous sand movement cycle than expected for present-day atmospheric pressure, and transport at lower speeds.

4. Mass Wasting and Slope Processes

4.1. Overview

Active Martian slope features can be divided into several categories (Table 2). Gullies are classically defined as features with alcoves, channels, and aprons resembling small terrestrial alluvial fans (Malin & Edgett, 2000). A variety of activity occurs in gullies, but in general, the landforms are created by many individual flow events. This contrasts with slope streaks (e.g., Sullivan et al., 2001) and recurring slope lineae (RSL; McEwen et al., 2011), which are relatively superficial features with little resolved topographic effect, although the latter often occur within small gully landforms and may contribute to their incision. Gully activity also differs from the formation of dune alcoves discussed in Section 5, which are larger than standard slipface grainflow source areas but smaller than the alcoves at the head of dune gullies, and which are commonly found in the north polar dunes and form in one event (Diniaga et al., 2019; Hansen et al., 2011). Additional categories of mass movement include rockfalls and small displacements of high-latitude rocks (e.g., Dundas, Mellon, et al., 2019).

An important characteristic of many fresh slope features is reflectance contrast with respect to surroundings. Throughout the following discussion in Section 4, features will be referred to as bright or dark relative to their surroundings to capture this distinction. It is important to note that this does not convey any information about absolute reflectance. For instance, slope streaks often appear very dark in images that are stretched to maximize contrast in the scene, but they normally occur in high-albedo dusty regions and their

absolute reflectance is considerably higher than RSL, which are also dark relative to their surroundings (McEwen et al., 2014).

4.2. Gullies

The Martian slope features with the most notable morphologic changes are gullies (Malin & Edgett, 2000). Mass movements in crater-wall gullies were first reported by Malin et al. (2006), who discovered two new relatively bright deposits with digitate termini. Later work has revealed dozens of additional changes in gullies throughout middle and high latitudes, allowing extensive analysis of modern gully activity.

Harrison et al. (2009), Diniega et al. (2010), and Dundas et al. (2010) showed that gully activity was seasonal, favoring cold seasons. Subsequent work (Dundas, Diniega, & McEwen, 2015; Dundas et al., 2012; Dundas, McEwen, et al., 2019; Raack et al., 2015, 2020; Vincendon, 2015) ultimately showed a strong temporal correlation with the presence of seasonal CO₂ frost, indicating that most present-day flows are driven by this frost. Northern hemisphere gullies are less active than those in the south, in addition to being less common, and the flows so far observed in the north have small geomorphic effects in most cases. Dundas, McEwen, et al. (2019) reported activity at 20% of monitored gully sites (each of which may include multiple gullies) in the south, but only 5% in the north, over typical monitoring intervals of 2–3 Mars years. These frequencies suggest activity recurrence intervals of decades to centuries for individual gullies (Dundas, Diniega, & McEwen, 2015). This hemispheric asymmetry has been attributed to the eccentricity of Mars' orbit, which results in a longer southern winter, although other hemispheric differences could be relevant (Dundas, Diniega, & McEwen, 2015; Dundas, McEwen, et al., 2019). Gullies at sites with RSL (Section 4.3) are more likely to be active than those at other locations, but this likely reflects a preference for steep slopes in both cases (Dundas, Diniega, & McEwen, 2015); RSL and gully flows have clearly distinct seasonality and morphology.

The brightness and color of flows in gullies is variable. The first two changes observed in gullies were brighter than the adjacent surface, and this was initially taken to be a characteristic of gully activity that could be used to interpret the cause (e.g., Heldmann et al., 2010; Malin et al., 2006; Williams et al., 2007). However, many later detections have been neutral or darker than their surroundings (Dundas, Diniega, & McEwen, 2015; Dundas et al., 2012; Dundas, McEwen, et al., 2019). Thus, the relative brightness of new gully flows does not appear to be a marker of the process. Additionally, some flows appear darker than their surroundings when imaged in shadow in the winter but have minimal contrast when illuminated the next summer; this is attributed to contrast with adjacent thin frost (Dundas, Diniega, & McEwen, 2015; Dundas et al., 2012). Flows can also be distinct in color while showing minimal broad-band albedo contrast in the HiRISE red channel (Dundas, Diniega, & McEwen, 2015), and in standard HiRISE enhanced-color products which assign blue-green, red, and near-infrared filter data to blue, green, and red colors for display (cf. Delamere et al., 2010) they are generally either blue or yellow relative to their surroundings (Dundas, McEwen, et al., 2019).

The morphological consequences of gully activity (Figure 4) can be large: although some flows are superficial and produce no topographic effects visible at the HiRISE scale, others substantially reshape the surface (Dundas, Diniega, & McEwen, 2015; Dundas et al., 2012; Dundas, McEwen, et al., 2019). Most flows have ill-defined or point-source origins, and the longest documented flow traveled over 2 km, although its observable effects were discontinuous (Dundas, McEwen, et al., 2019). Channels are extended and modified in some cases, and the interior channel morphology is commonly re-worked (Dundas, Diniega, & McEwen, 2015; Dundas, McEwen, et al., 2019). Sinuous channel bends can form, migrate, and straighten or become cut off (Dundas, McEwen, et al., 2019; Pasquon, Gargani, Massé, et al., 2019). Collapse of channel sidewalls occurs following flow passage, as does incision and infill within existing channels, producing apparent terraces (Dundas, Diniega, & McEwen, 2015; Dundas, McEwen, et al., 2019). Many gullies are incised into mantling materials (e.g., Christensen, 2003), which in many cases likely have a high H₂O ice content because the total apron volumes are smaller than the eroded alcoves (Conway & Balme, 2014; Gulick et al., 2019). Khuller and Christensen (2021) documented exposure of bright material interpreted as water ice by slumping in several alcoves.

Although Malin et al. (2006) attributed formation of the first two detected bright flows to liquid water; Pelletier et al. (2008) showed that one of the new deposits had a morphology and extent consistent with a

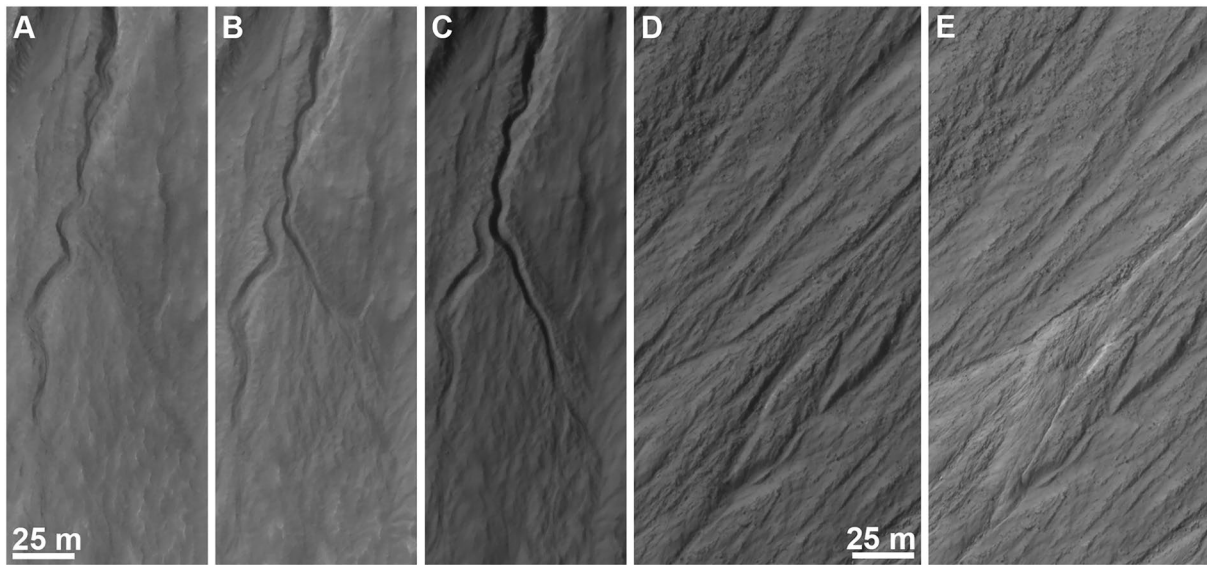


Figure 4. Examples of morphologic changes in nondune gullies. (a–c) Multi-stage incision of a new channel section in Dunkassa crater via several flows. (d and e) Thick lobate deposit filling and partially burying a channel segment in Selevac crater ((a): Subsection of High Resolution Imaging Science Experiment [HiRISE] image ESP_013115_1420 [Mars Year, MY 29, $L_S = 266^\circ$]. (b): Subsection of HiRISE image ESP_032011_1425 [MY 31, $L_S = 325^\circ$]. (c): Subsection of HiRISE image ESP_055496_1420 [MY 34, $L_S = 184^\circ$]. (d): Subsection of HiRISE image ESP_028622_1425 [MY 31, $L_S = 166^\circ$]. (e): Subsection of HiRISE image ESP_055443_1425 [MY 34, $L_S = 182^\circ$]. North is up and illumination is from the left in all panels).

dry flow. Modeling of new gully flows in Hale crater demonstrates that they are fluidized to a degree that resembles terrestrial debris flows (de Haas et al., 2019). While this result is consistent with liquid water, it could also be explained by vaporization of CO_2 frost within the flow (de Haas et al., 2019).

Although gullies on sand dunes are frequently treated separately from those on crater walls and other slopes, the morphologies are often similar. Formation of a new dune gully channel was reported based on MOC images (MGS MOC Release MOC2-1220, 2005), and gully formation constrained to specific Mars seasons has been identified in HiRISE images (Dinięga et al., 2010; Dundas et al., 2012). Dune gullies appear to be more active, likely because the substrate is weaker (Dinięga et al., 2010; Dundas, Dinięga, & McEwen, 2015; Dundas et al., 2012; Dundas, McEwen, et al., 2019; Pasquon, Gargani, Massé, et al., 2019; Pasquon, Gargani, Nachon, et al., 2019). This translates to more frequent flows and larger morphologic effects, including formation of entire large gullies or gully segments (Dundas et al., 2012; Dundas, McEwen, et al., 2019) and more significant changes to channel sinuosity (Pasquon, Gargani, Massé, et al., 2019). Some individual gullies are even active annually. Massive channel incision can occur, with one channel in a large gully in Matara crater widening from 30 to 60 meters over the course of a Mars year (Pasquon, Gargani, Massé, et al., 2019). Dune and nondune gullies have similar activity timing driven by seasonal frost (Dinięga et al., 2010; Dundas et al., 2012). Pasquon, Gargani, Nachon, et al. (2019) conducted a more detailed analysis of dune gully activity in Kaiser crater and divided it into multiple types, with fine digitate flows occurring in autumn and winter, but larger flows only occurring in late winter.

Some dune gullies do have an unusual morphology, sometimes characterized as “linear,” with minimal alcoves and terminal deposits, and commonly with detached terminal pits (Mangold et al., 2003; Reiss & Jaumann, 2003). Development of such features is associated with the end of spring defrosting, as was first reported in Russell crater (Reiss et al., 2010). Late-winter and early spring activity appears to be typical of linear dune gullies (Dinięga et al., 2013; Jouannic et al., 2019; Pasquon et al., 2016; Pasquon, Gargani, Nachon, et al., 2019). The surface changes include formation of new channels and extension of existing channels sometimes exceeding 500 m in length, although <100 m was more common for individual events (Pasquon et al., 2016). Dundas et al. (2012) reported blocks of CO_2 ice with associated dark halos near the termini of some linear gullies, and Dinięga et al. (2013) argued that such channels form via sliding slabs of CO_2 ice, with ice block mobility enhanced by lifting due to basal sublimation. Dinwiddie and Titus (2021) reported airborne plumes sourced from the channels in Russell crater near $L_S = 200^\circ$, similar to the time

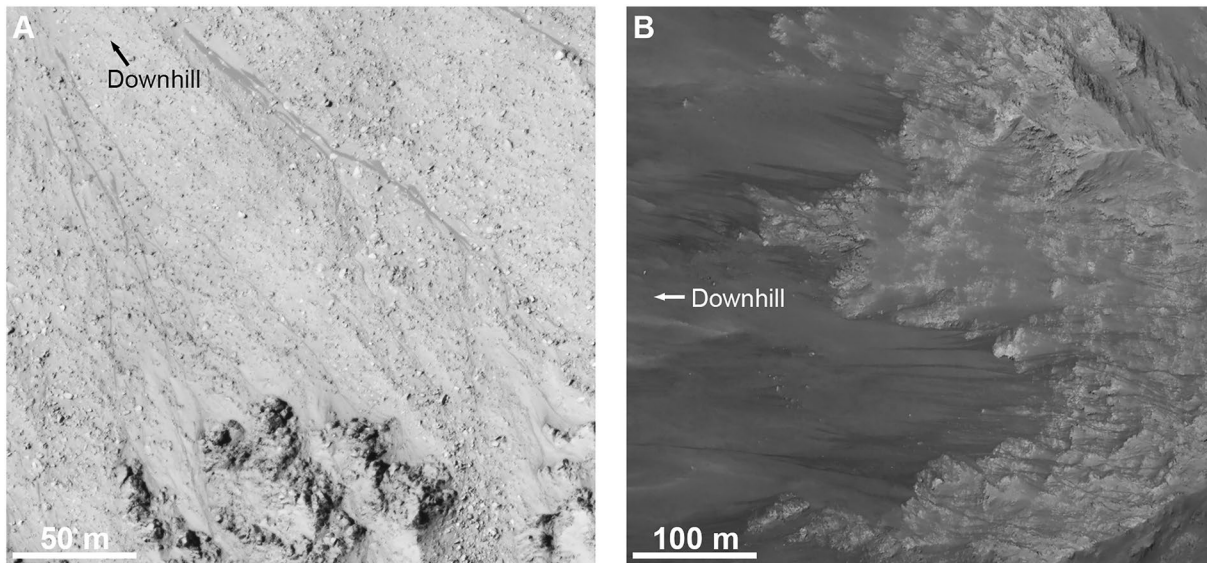


Figure 5. Recurring slope lineae in Raga crater (a) and Coprates Chasma (b) ((a): Subsection of High Resolution Imaging Science Experiment [HiRISE] image ESP_014011_1315. (b): Subsection of HiRISE image ESP_059476_1670. North is up and illumination is from the left in both panels).

when blocks were observed. Formation of new terminal pits is also occurring (Diniega et al., 2013; Dundas et al., 2012; Pasquon et al., 2016; Pasquon, Gargani, Nachon, et al., 2019), likely due to sublimation of these blocks. Detached pits could result from blocks bouncing and overshooting the gully terminus, or by impact of granular material from gas jets ejected by blocks at the terminus (Mc Keown et al., 2017). Defrosting spots and flows similar to those seen at high latitude (Section 5.1) also occur, generally preceding the larger morphologic changes (e.g., Gardin et al., 2010). Small-scale defrosting spots associated with sublimating CO₂ appear around the Russell crater dune gullies from around $L_s = 105\text{--}205^\circ$ and develop into flows (Dinwiddie & Titus, 2021; Jouannic et al., 2019).

In aggregate, it appears that the morphology of gullies is currently being shaped by modern CO₂ frost processes, although a few studies still explore whether brines may be involved in the present-day activity of linear dune gullies (e.g., Jouannic et al., 2019) and Khuller and Christensen (2021) suggested that melting in alcoves could occur in association with bright exposures. Dune gullies are so active that they must entirely form on timescales much less than obliquity cycles, and indeed a few new or completely redeveloped gullies are observed to form on sand dunes within a few Mars years (Dundas et al., 2012; Dundas, McEwen, et al., 2019). On less-mobile nonsand substrates, formation proceeds more slowly. The present-day activity appears capable of forming the observed nondune gullies when integrated over \sim Myr timescales (Dundas, McEwen, et al., 2019), but it is still debated whether other processes such as aqueous debris flows or snow-melt also contributed to their formation under past climate conditions (e.g., Conway et al., 2019; Khuller & Christensen, 2021).

4.3. RSL and Slumps

RSL (Figure 5) were initially described by McEwen et al. (2011, 2014). RSL are relatively dark flows on steep slopes in the low-albedo regions of Mars, typically meters wide and tens to hundreds of meters long. Upon discovery, they were interpreted as possible evidence of liquid water or brine (McEwen et al., 2011). They characteristically exhibit incremental growth over a period of several months, fade annually, and recur in approximately the same locations. Many hundreds of possible and confirmed RSL sites have been mapped, primarily in the southern midlatitudes, Valles Marineris, and Chryse and Acidalia Planitia (Stillman, 2018; Stillman & Grimm, 2018; Stillman et al., 2014, 2016, 2017; McEwen et al., 2021; Ojha et al., 2014). RSL are generally active in warm seasons (McEwen et al., 2011, 2014; Ojha et al., 2014; Stillman et al., 2014), and they were more active and widespread immediately following planet-encircling dust events (PEDEs)

(McEwen et al., 2011, 2021; Stillman et al., 2014). Some lineae have similar morphology but different temporal behavior (e.g., Dundas, 2020a; McEwen et al., 2014).

Some spectral information helps to constrain the nature of RSL. Ojha et al. (2013) observed spectral changes over time that they interpreted to indicate changes in the surface grain size during the RSL active season. Ojha et al. (2015) also reported a detection of hydrated oxychlorine salts associated with activity at several RSL sites, but this appears to have been a data-processing artifact (Leask et al., 2018; Vincendon et al., 2019). Liquid water should markedly affect the thermal conductivity of the ground, but Edwards and Piqueux (2016) observed no thermal signature for RSL in Garni crater and placed an upper limit of 3 vol% on the water content at the times and places of Thermal Emission Imaging System (THEMIS; Christensen et al., 2004) observations of that site. However, none of those observations occurred during a year and season when RSL were known to be present with sufficient areal coverage for THEMIS detection (Stillman et al., 2017).

As seen from orbit, RSL produce only changes in relative brightness, without resolvable topographic effects (Chojnacki et al. (2016) reported some topographic changes near but not in lineae, discussed below). McEwen et al. (2014) quantified the surface darkening associated with some RSL; after atmospheric correction, the lineae in Palikir crater were ~20% darker than adjacent fan surfaces. Schaefer et al. (2019) found similar values with a simpler atmospheric correction at Tivat crater and found that RSL had similar brightness and fading timescales to nearby rockfall tracks. They suggested that this indicated that RSL fade because dust is removed from the surroundings, rather than because of local brightening of the lineae.

The Color and Stereo Surface Imaging System (CaSSIS; N. Thomas et al., 2017) can observe the Martian surface at any time of day due to the nonsun-synchronous orbit of the Trace Gas Orbiter (TGO). Munaretto et al. (2020) used CaSSIS images to show that there is no detectable difference in the relative albedo of RSL and surroundings between the morning and the afternoon; such a difference would be expected for wet flows due to evaporation during the day. The morning observation was at 11 a.m., potentially too late and warm to see darkening from still-wet flows (N. Thomas et al., 2017).

The slopes of RSL provide an important constraint on their formation. From the outset, they were noted to occur on steep slopes (Chojnacki et al., 2016; McEwen et al., 2011; Ojha et al., 2014). Dundas et al. (2017) then showed evidence that the terminal slopes of RSL are all at approximately the angle of repose for sand, suggesting that they are dry granular flows. Tebolt et al. (2020) reported some slopes above and below the angle of repose, but some measurement locations indicated therein do not appear to correspond to RSL. Stillman et al. (2020) and Munaretto et al. (2020) independently found that RSL occur on angle-of-repose slopes, within measurement uncertainties.

The originally observed RSL recur and fade with an annual cycle, and annual fading and recurrence remains part of the definition of McEwen et al. (2014). However, there are slope lineae with other temporal behaviors. These include lineae that have two active seasons or pulses of activity, persist for several Mars years, do not recur, exhibit incomplete fading each year, and/or are active in cold seasons (Dundas, 2020a; Dundas & McEwen, 2015; Stillman, 2018; Stillman & Grimm, 2018; Stillman et al., 2017; Ojha et al., 2014). Dundas (2020a) accordingly suggested that RSL are a subset of lineae that have annual cycles and growth and fading, and that other lineae may be driven by the same processes but with different growth or fading timescales.

The gradual extension of RSL is similar to seeping water and can be successfully fit by seepage models (Grimm et al., 2014; Levy, 2012). However, the source of putative water remains unknown. Stillman et al. (2016, 2017), Stillman and Grimm (2018), and Abotalib and Heggy (2019) have proposed release of deep groundwater. However, RSL occur on isolated topographic highs where deep crustal groundwater release is unlikely, including in Valles Marineris where bounding faults would likely direct any groundwater release to the trough floor (Chojnacki et al., 2016; McEwen et al., 2011, 2014). The atmospheric water content is low, so any atmospheric source must be very volumetrically limited, and peaks in seasonal H₂O column abundances do not correlate or anticorrelate with RSL activity (McEwen et al., 2014). Atmospheric resupply of shallow aquifers is similarly implausible since water should be removed from warm RSL slopes rather than deposited there (Dundas et al., 2017). Salty solutions could reduce these issues but RSL slopes lack the large salt deposits that would be expected from persistent springs (Dundas et al., 2017).

Recently, several workers have proposed models involving little or no water. Dundas et al. (2017) argued that RSL are granular flows, but they did not present a detailed model for RSL initiation and left open the possibility that water was involved in some way. More recently, Schaefer et al. (2019) and Vincendon et al. (2019) proposed entirely dry hypotheses for RSL formation involving mobilization of surface dust, while Dundas (2020a) argued that they are aeolian-driven sand flows made visible by the absence of a dust coating on fresh flows. The great abundance of RSL and associated dust devil tracks following the 2018 PEDE suggest that dust lifting may initiate RSL formation (McEwen et al., 2021).

Chojnacki et al. (2016) and Ojha et al. (2017) described slumps occurring at some RSL sites in Valles Marineris. The slumps form in spring or early summer on the same slopes as RSL and have similar brightness and color. However, they initiate near RSL termini. They are typically larger and wider than the nearby RSL and involve resolvable mass movement producing headscarps and lobate toes. The seasonality of activity appears to be distinct from RSL, although the number of sites and individual flows is currently small. At a well-studied site in Juventae Chasma, slumps generally formed between $L_S = 345\text{--}120^\circ$ (Ojha et al., 2017), beginning around the season when RSL on the same slopes cease activity. A connection to RSL thus appears possible but is not yet fully understood. Alternatively, because the slumps do not occur at most RSL sites, the co-occurrence could be a coincidence if the necessary conditions for slumps are simply a subset of a much broader set of conditions permitting RSL.

4.4. Slope Streaks

Slope streaks (Figure 6) are one of the longest-known active slope features on Mars, first observed in Viking Orbiter data (Morris, 1982). They are found in dusty, high-albedo regions, and typically have a roughly triangular shape that spreads downhill from a point source. Most are darker than their surroundings, but bright streaks also occur. They are distinguished from RSL by several factors: slope streaks form in bright, dusty regions, usually persist for many years, and do not grow incrementally. They are also commonly wider, with the wedge shape contrasting with narrow lineae.

New slope streaks were first observed in MOC images, and it was quickly noted that the new streaks were always darker than existing streaks, indicating that they fade over time (Sullivan et al., 2001). Aharonson et al. (2003) conducted a survey of 173 collocated image pairs and found that the rate of formation of new streaks was $\sim 7\%$ per existing streak, per Martian year, and apparently exceeded the rate of streak fading. Schorghofer et al. (2007) examined a small number of sites and found a formation rate of 3%, again exceeding the rate of disappearance. Bergonio et al. (2013) found a balance between formation and erasure, but only at one site. This discrepancy could be explained if erasure is at least partially stochastic (Aharonson et al., 2003). Individual streaks form rapidly, within days (Dundas et al., 2017; Heyer et al., 2018) and possibly much faster, and then do not evolve further other than fading slowly. Existing streaks can prevent propagation of new streaks, but overprinting does occur occasionally (Dundas, 2020b; Sullivan et al., 2001). The seasonality of slope streak formation has been debated. Schorghofer and King (2011) examined three sites and found sporadic formation throughout the year, but Heyer et al. (2019) reported a preference for formation in the autumn. Dundas (2020b) noted that streak formation sometimes occurred in concentrated bursts that may have favored seasons but also substantial year-to-year variation in rates; Schorghofer and King (2011) also reported formation of clusters of streaks.

Most slope streaks are darker than their surroundings by up to 10% (Sullivan et al., 2001), but streaks that are up to 2% brighter than surrounding terrain also occur (e.g., Figure 6d) (Sullivan et al., 2001). Bright streaks are most common in Arabia Terra, where the formation of new dark slope streaks is slow, and a strong negative correlation was found between the number of bright slope streaks and the number of new dark slope streaks annually (Schorghofer et al., 2007). New bright streaks have so far not been definitively observed, and Schorghofer et al. (2007) suggested that they might form as an evolutionary stage of dark streaks. Valantinas et al. (2019, 2020) have reported new bright streaks but it is uncertain whether they indicate new flows or evolution and exhumation of existing flow features. Further, it is possible that under certain observing conditions, such as high atmospheric opacity or high solar incidence angles (for which signal-to-noise ratio is low), bright slope streaks could be present but not visible. This means that a false detection of new bright slope streaks could occur if a location is first observed with low SNR and shows no evidence of bright slope streaks but is later observed under better conditions and displays bright slope streaks.

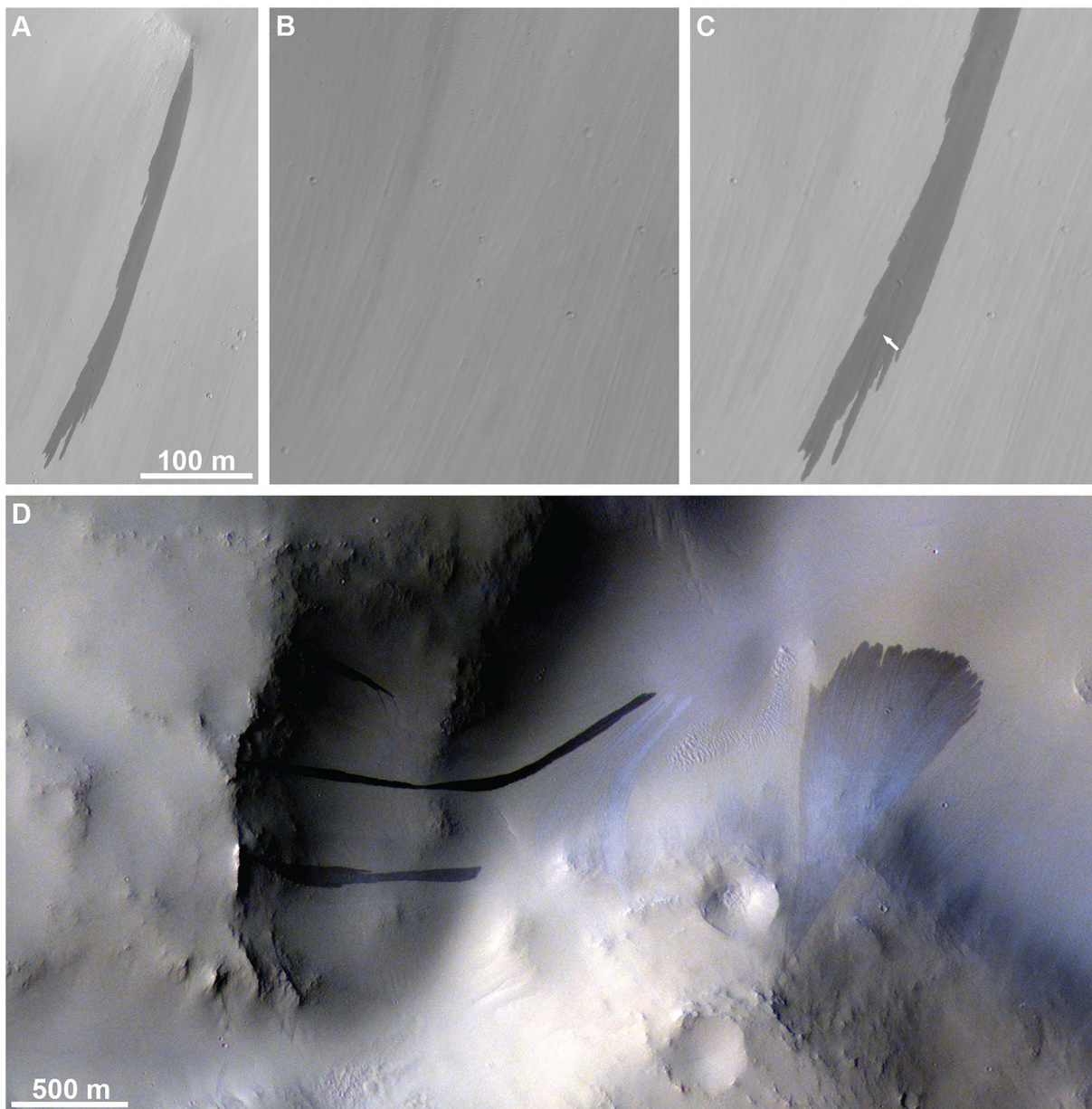


Figure 6. Example of a new slope streak (a and c) and various dark and bright streaks observed in Arabia Terra. (a) shows the full extent of the streak including the point source. (b and c) are before-and-after images showing the toe of the streak with identical resolution and very similar lighting. Many small topographic features within the streak are preserved, indicating minimal change in surface topography; arrow indicates a ridge, demonstrating topographic change. Similar features outside the streak are unchanged. (d) exhibits dark streaks (left), bright streaks (center), and a slope streak with dark and bright areas (right). Both dark and bright streaks are visible under the same illumination conditions, indicating that their brightness differences are independent of the viewing geometry ((a and c): Subsections of High Resolution Imaging Science Experiment [HiRISE] image ESP_028616_1920 [Mars Year, MY 31, $L_s = 165^\circ$]. (b): Subsection of HiRISE image PSP_008441_1920 [MY 29, $L_s = 72^\circ$]. (d): Subsection of Colour and Stereo Surface Imaging System image MY35_009504_159_0. North is up and illumination is from the left in all panels).

Observations with the Compact Reconnaissance Imaging Spectrometer for Mars (CRISM; Murchie et al., 2007) found spectrally featureless darkening of dark slope streaks in the near-infrared ($\sim 1\text{--}3.5\ \mu\text{m}$; Amador et al., 2016; Mushkin et al., 2010). Mushkin et al. (2010) then concluded that slope streak darkening is due not to an exposure of the pre-existing substrate, but to soil enrichment of low-albedo ferric oxides. Using thermal infrared data, Schorghofer et al. (2007) found that some dark slope streaks appear warmer than their surroundings by 4 K in afternoon THEMIS-IR images. They suggested that these higher temperatures

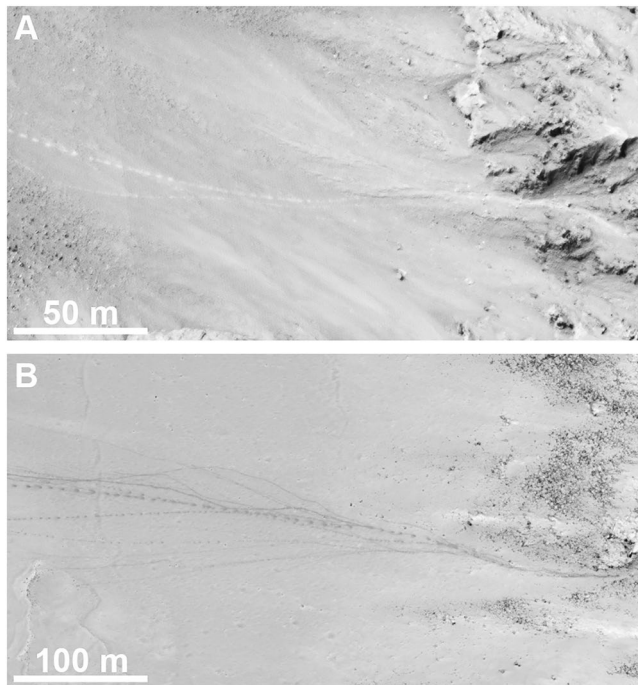


Figure 7. Examples of rockfalls that are brighter (a) and darker (b) than their surroundings. Note discontinuous nature indicating bouncing of the falling rocks, and division into multiple tracks ((a): Subsection of High Resolution Imaging Science Experiment [HiRISE] image ESP_026493_1690. (b): Subsection of HiRISE image ESP_036261_1705. North is up, illumination is from the left, and downhill is to the left in both panels).

could be related to different thermophysical properties of the slope streak surface, such as a lower thermal conductivity.

Slope streaks clearly favor steep slopes. Brusnikin et al. (2016) found that slopes at the streak origin were variable but that streaks could only initiate on slopes above 20° . However, the terminal slope where the streak halted was highly variable: some matched the initiation slope, while others reached horizontal surfaces. No uphill flow was observed over long baselines, but over short baselines, streaks can surmount or circumvent small obstacles. Bhardwaj et al. (2017) proposed low-slope origin areas for some streaks but examined very short baselines where slopes derived from HiRISE Digital Terrain Models may not be reliable because small absolute errors result in large slope errors.

Some slope streaks have clearly identifiable triggers, such as rockfalls, impact craters, or dust devils (Chuang et al., 2007; Dundas, 2020b; Heyer et al., 2020; Malin & Edgett, 2000). However, the vast majority lack an identifiable trigger (Dundas, 2020b; Heyer et al., 2020). Proposed explanations for this include triggering by winds or by insolation-driven gas flow (Dundas, 2020b; Heyer et al., 2020).

Chuang et al. (2010) reported one new slope streak with topographic relief along its edge. Getting more thorough evidence for the topographic effects of slope streaks has only been possible with HiRISE-to-HiRISE image comparisons. Dundas (2020b) reported that the vast majority of streaks do not have topographic effects that are visible to HiRISE, and small-scale topography is often preserved within the streak; even among large streaks >500 m long, only 4% resulted in observable changes to the surface morphology. This indicates that the streak-forming flows are typically superficial, but do involve material transport. The darkening of slope streaks does not appear to be the result of exposure of a darker substrate and may instead be due to surface roughness or grain size effects (Baratoux et al., 2006).

Wet or dry origins for slope streaks have been extensively debated. Bhardwaj et al. (2019) provided a review of much of this debate, which is not repeated here, but they did not reach a strong conclusion. However, several very recent sets of observations have strongly favored dry origins, such as dust avalanches (Dundas, 2020b; Heyer et al., 2020).

4.5. Other Slope Changes

New tracks from rockfalls (Figure 7) have been observed in HiRISE and MOC images (Dundas, Mellon, et al., 2019; MGS MOC Release MOC2-1222, 2005; Schaefer et al., 2019). The tracks are commonly discontinuous, likely due to bouncing of the falling rocks as they descend the slope. New tracks may be brighter or darker than their surroundings, and well-resolved tracks often do not terminate at a visible boulder, indicating that the impact markings are wider than the falling rock. Study of rockfalls in general suggests that they are largely induced by thermal stress (Tesson et al., 2020), which may be testable by future observations that constrain the timing of falls. Isolated falls could also be triggered by seismic activity (J. R. Brown & Roberts, 2019; Kumar et al., 2019; Roberts et al., 2012). Although timing constraints have not been documented for many rockfalls, they are expected to be rapid events, as their discontinuous nature implies a rapidly falling, bouncing rock.

M. F. Thomas et al. (2020) reported numerous surface changes on equatorial sulfate-rich sedimentary deposits, which are weak and should be prone to mass wasting. These include some extensive mass movements with large topographic effects. These may be similar to rockfalls, but with larger effects due to the weak substrate.

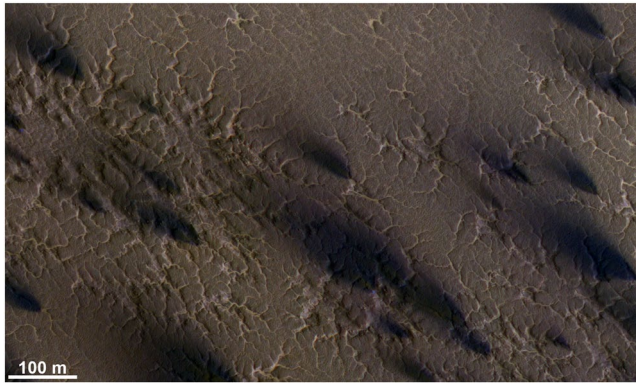


Figure 8. Fan deposits (dark patches) and araneiform landforms near the south pole. The deposits appear dark because they are composed of lithic material which contrasts with surface frost, and exhibit no contrast after the frost sublimates (Subsection of High Resolution Imaging Science Experiment image ESP_055604_0930. North is to the lower right and illumination is from the upper right).

Small-scale movement of dozens of rocks has been observed in high-latitude craters (Dundas, Mellon, et al., 2019). These shifts are commonly, but not uniquely, associated with decameters-scale arcs and lobes of sorted rocks, and could be contributing to the formation of those landforms. These movements are unlike energetic bouncing rockfalls: they can occur on slopes below the angle of repose and generally only cause shifts of a few meters, consistent with a low-energy process. The seasonal timing of this activity has not been well constrained, but at least two movements were documented to have occurred when seasonal frost was absent.

Viking Lander 1 observed two new small slump features that formed on dust drift deposits over the course of the mission (Guinness et al., 1982; Jones et al., 1979). Moore et al. (1987) described the failures, which both occurred in late summer roughly one Mars year apart. Moore et al. (1987) proposed that the failures were due to generation of positive gas pore pressure, while Jones et al. (1979) suggested that they were due to wind-induced shear failure. Similar small failures of dusty, crusted material have been observed in Gale crater by *Curiosity* along with flow of the underlying sand (Dickson et al., 2016).

Polar avalanches and blockfalls are common and discussed in more detail in Section 5.2.

5. Periglacial and Polar Processes

The polar regions of Mars exhibit several distinctive processes. Although some of these overlap with other categories, they are discussed separately here.

5.1. Defrosting and Sublimation Processes

The seasonal CO₂ ice caps on Mars exhibit active gas-venting processes during spring (Hansen et al., 2010; Kieffer, 2007; Kieffer et al., 2006; Piqueux et al., 2003). Translucent, impermeable slab ice sublimates at its base due to a solid-state greenhouse effect, resulting in the buildup of gas pressure beneath the seasonal ice. In the southern hemisphere, sub-ice gas flow and venting mobilizes surface material into fan deposits over the ice and is thought to create a variety of landforms that have been dubbed “spiders” or araneiform terrain (Figure 8) (e.g., Hansen et al., 2010; Piqueux et al., 2003). Brine flows have been proposed as an alternative to these frost phenomena for several features discussed below (Kereszturi et al., 2009, 2010, 2011), but the depressurization model is favored, primarily because of the low condensation temperatures of CO₂ frost (Hansen et al., 2013).

Spots and fans of fine-grained material deposited on the seasonal ice layer by the escaping gas are abundant every spring, but in most locations they disappear after there is no longer surface ice to provide reflectance contrast (Piqueux & Christensen, 2008; Piqueux et al., 2003; Portyankina et al., 2010; N. Thomas et al., 2010). Deposition of material on top of frost shows that this is an active material-transport process, which manifests as both ballistically emplaced spots and fans and ground-hugging flows (Hansen et al., 2010; N. Thomas et al., 2010). These deposits must be sufficiently thick as to change the albedo and thermal properties (at least 0.5 mm, depending on grain size; Piqueux & Christensen, 2008). Once defrosted, changes to the surface morphology are mostly imperceptible for available image resolutions and time baselines, but there are exceptions. Several examples of new or growing converging dendritic troughs have been described on sandy surfaces in the southern hemisphere (Portyankina et al., 2017). Although small in scale, these demonstrate ongoing development of the landforms, with new troughs that are tens of meters long and tens of centimeters wide. The dendritic troughs resemble small araneiforms and likely reflect the same process in a more mobile substrate. The formation timescale of well-developed araneiforms has been estimated to be $>10^4$ years (Piqueux & Christensen, 2008).

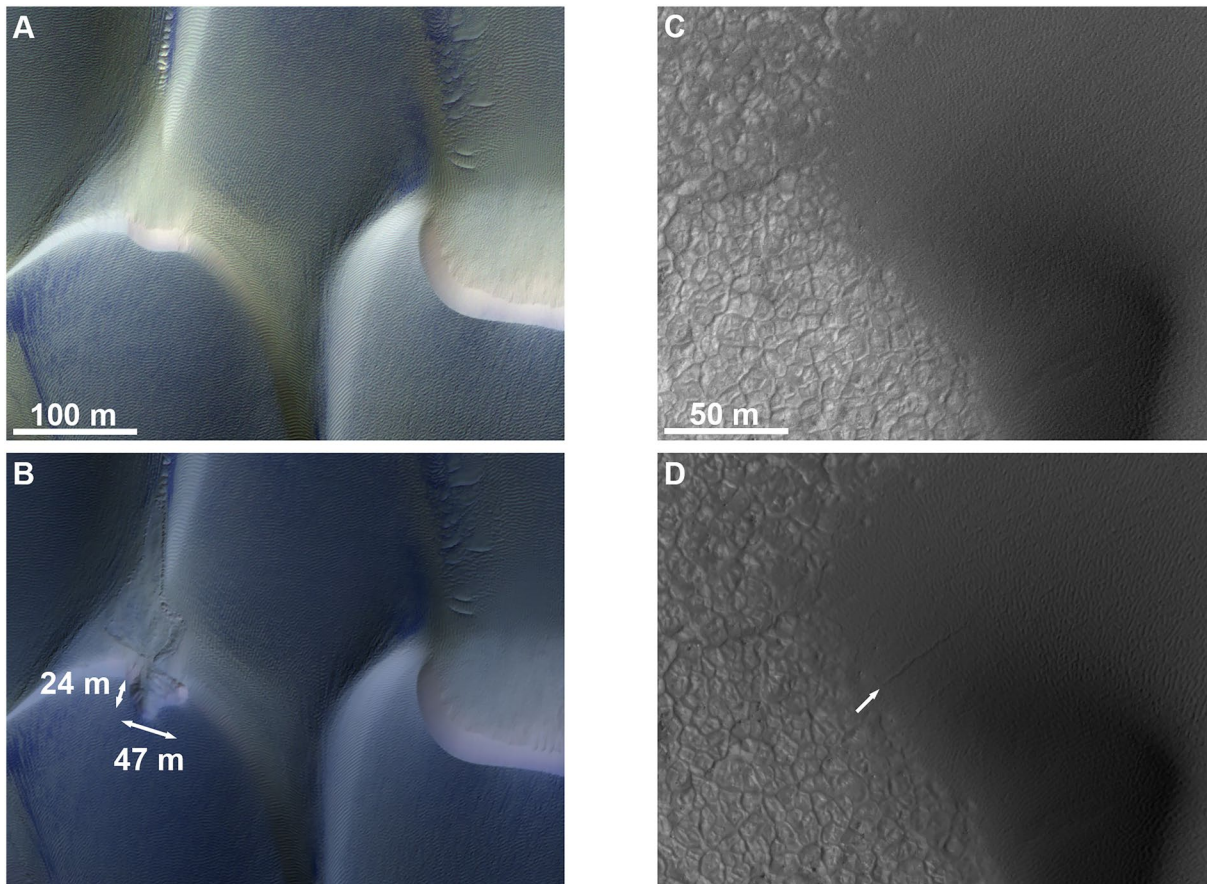


Figure 9. Changes in sand dunes in the north polar erg. (a and b) Formation of a decameter-scale alcove on a dune slip face. (c and d) Formation of a furrow ((a): Subsection of High Resolution Imaging Science Experiment [HiRISE] image ESP_027394_2640 [Mars Year, MY 31, $L_S = 118^\circ$]. (b): Subsection of HiRISE image ESP_036387_2640 [MY 32, $L_S = 124^\circ$]. (c): Subsection of HiRISE image PSP_009439_2600 [MY 29, $L_S = 106^\circ$]. (d): Subsection of HiRISE image ESP_18445_2600 [MY 30, $L_S = 113^\circ$]. North is to the right and illumination is from the upper right in (a/b), and north is to the lower left and illumination is from the right in (c/d).

The dunes of the north polar erg exhibit extensive activity, combining vigorous aeolian transport in summer (Bridges, Bourke, et al., 2012; Chojnacki et al., 2019), with seasonal frost effects in the winter (Diniega et al., 2019; Hansen et al., 2011, 2013, 2015). When the sun comes up in the spring, a gas-venting process similar to that in the south takes place, albeit on the mobile sand dunes of the north polar erg. The seasonal layer of ice is observed to crack along the crest of the dunes, in large polygons on the shallow slopes of the stoss side of the dunes, and around the dune-interdune surface interface (Hansen et al., 2013; Portyankina et al., 2012), releasing sand with the escaping gas through cracks in the ice and forming furrows. Another observed landform modification is new alcoves at the crest of the dunes (Figures 9a and 9b). Unlike gullies, these features rarely have channels, just the alcove and associated debris apron. The driver for formation of the new alcoves, which can be tens of meters across and cut back meters from the brink of the dune, has been proposed to be (a) associated with sublimation of seasonal ice (Hansen et al., 2010); (b) wind-driven grainflow (Horgan & Bell, 2012); (c) snowfall (Hansen et al., 2018; Hayne et al., 2016); and/or (d) processes associated with the initial condensation of seasonal ice (Hansen et al., 2015). Ground-hugging defrosting flows are observed to occur within dune alcoves (Hansen et al., 2011, 2013, 2015) but may not be responsible for forming them. Seasonal monitoring demonstrates that the alcoves form in fall or winter, when frost is present; most timing constraints are loose, but one alcove was demonstrated to form between $L_S = 169\text{--}191^\circ$ during the earliest stage of frost condensation (Diniega et al., 2019). This supports a model where alcoves primarily form in autumn due to loading as the frost initially condenses, are enhanced by spring sublimation activity, and then are erased by standard aeolian activity during the frost-free season (Diniega et al., 2019).

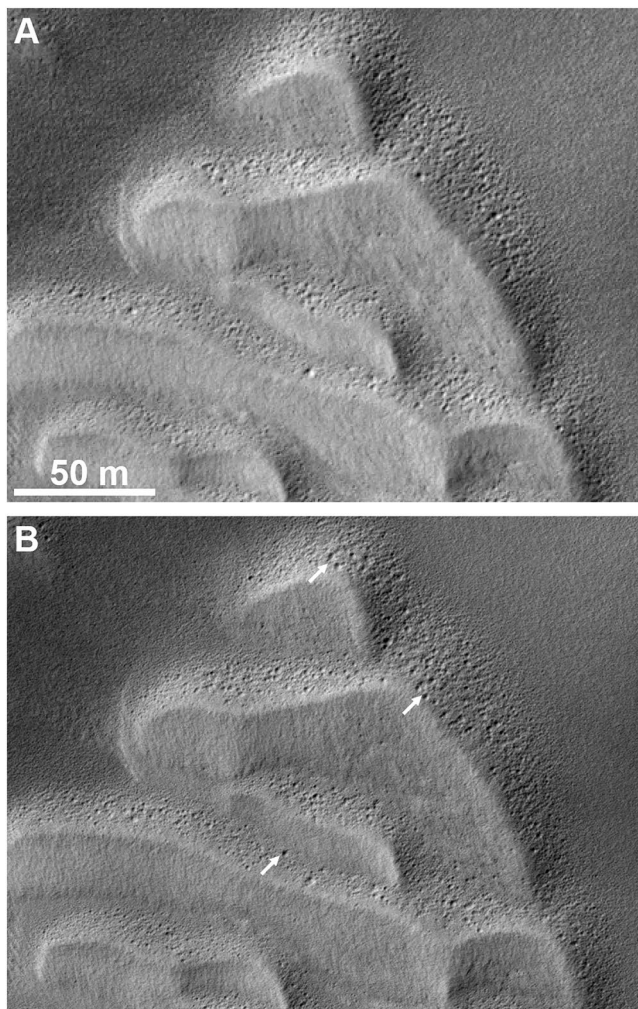


Figure 10. (a and b) Evolution of pit fields via formation of pits on aeolian bedforms at 55.4°S. Arrows indicate the largest of many new pits ((a): Subsection of High Resolution Imaging Science Experiment [HiRISE] image ESP_040428_1245 [Mars Year, MY 32, $L_S = 307^\circ$]. (b): Subsection of HiRISE image ESP_058019_1245 [MY 31, $L_S = 305^\circ$]. The former image has a coarser pixel scale than the latter and has been enlarged 2× for easy comparison. North is up and illumination is from the left).

Furrows (Figures 9c and 9d) observed on northern hemisphere dunes are associated with seasonal fans and likely form via gas flow processes in a manner similar to southern hemisphere araneiform features (Bourke, 2013; Hansen et al., 2013). Furrows are visible every summer when seasonal ice has sublimed, sometimes but not always in the same location, showing that wind and frost reshape a substrate of mobile sand (Bourke, 2013; Hansen et al., 2012). The furrows can be tens of meters long and tens of centimeters deep (Bourke, 2013). The greater geomorphic change in the furrows compared with the southern hemisphere dendritic troughs and araneiform terrain likely reflects a spectrum of substrate mobility from unconsolidated sand (furrows) to more cohesive material (araneiforms).

Changing pits that are likely associated with seasonal frost are also observed in some bedforms at high southern latitude (Figure 10). In this case, the bedforms are brighter than their surroundings, which may indicate that their surface material mineralogy is not the common basaltic sand, which is typically the darkest material in an image. Migration of those bedforms has not been detected but new pits on the side of the bedforms do occur. These likely reflect the sublimation activity, as they resemble terminal pits at the end of linear gullies, but they have not been studied in detail.

In addition to the seasonal caps of CO₂ frost, both poles have residual caps of bright ice that persist through the summer. The south polar residual cap consists of a thin (~10 m) veneer of CO₂ ice overlying H₂O ice (Bibring et al., 2004; Byrne & Ingersoll, 2003; Titus et al., 2003), variably eroded by round pits that have led this surface to be dubbed “Swiss Cheese” terrain. Malin et al. (2001) observed that these pits were expanding due to insolation-driven sublimation of the walls (Figure 11). The most detailed measurements of expansion to date show wall and scarp retreat rates of 2–5 m/MY, implying pit ages of decades to centuries (P. C. Thomas et al., 2016). Dust fallout from southern-summer PEDE can darken the residual cap except adjacent to vigorously sublimating pit walls, which leads “bright halos” to appear around the pits soon after a dust storm. The disappearance of these halos indicates net burial of the dusty layer with CO₂ ice in the winters after large storms (Becerra et al., 2015), and it is likely that this CO₂ deposition compensates for some of the pit erosion. It remains uncertain whether the cap is in a net steady state or undergoing aggradation or retreat (P. C. Thomas et al., 2016).

The north polar residual cap is large-grained, mostly dust-free H₂O ice (Kieffer, 1990; Langevin et al., 2005). Seasonal observations of H₂O-ice spectral features indicate a transition from net sublimation to condensation in mid-summer, with a layer averaging approximately 70 microns thick deposited in late summer, although the thickness was spatially variable (A. J. Brown et al., 2016). Changes in the north polar residual cap occur both seasonally and inter-annually as the shape of high-albedo features evolves, demonstrating variable accumulation and removal of a thin coating of surface dust (Calvin et al., 2015). However, the extent to which these changes are causing long-term evolution of the cap is unknown. Interannual change in the extent of the north polar residual cap during MY 24–27 was small and reversible on timescales of 1 or 2 Mars years (Byrne, Zuber, & Neumann, 2008). The surface of the north polar residual cap has a young crater-retention age, consistent with either a recent resurfacing event or active resurfacing that places the crater population in equilibrium with a very young age (Landis et al., 2016). Changes in the distribution of frost and ice within small craters have been observed, although their significance remains unclear since both deposition and removal occurs,

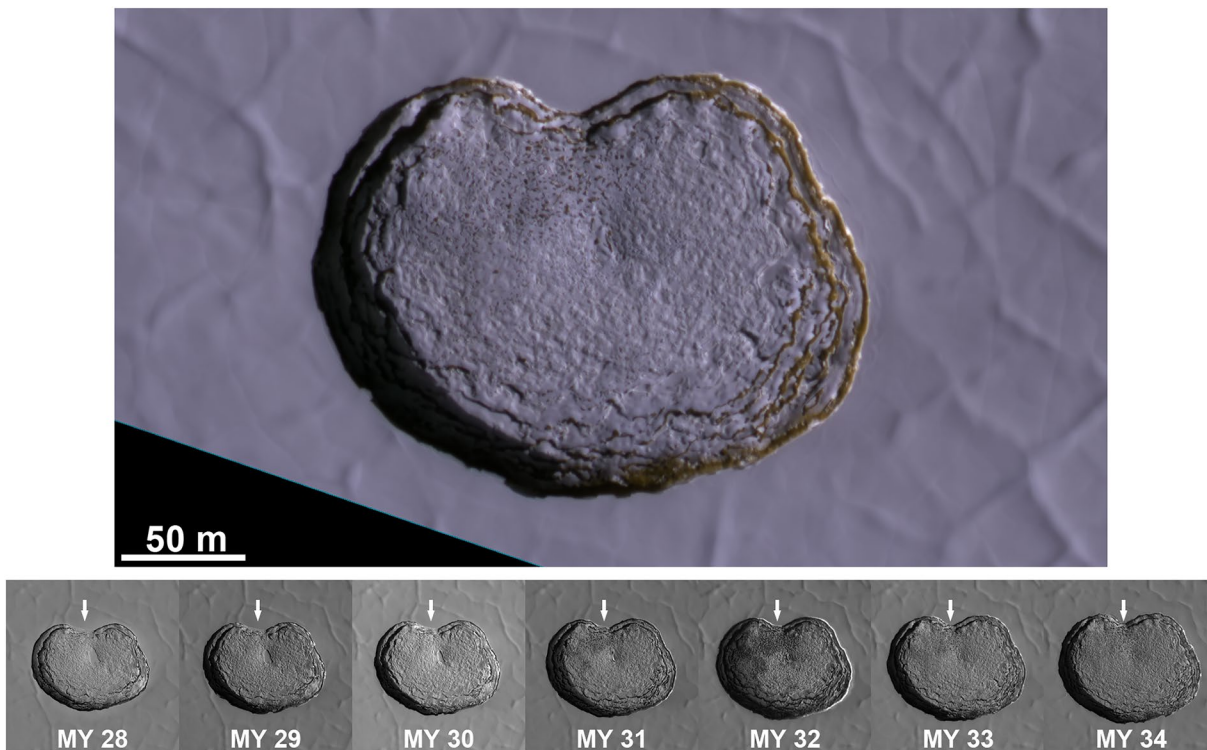


Figure 11. Expanding pit in the south polar residual cap. The upper panel shows a full-resolution view of a pit; the lower sequence shows growth of the pit across seven Mars years. Arrow indicates common location in all panels (Top: Subsection of High Resolution Imaging Science Experiment [HiRISE] image ESP_058026_0930. Bottom: Subsections of HiRISE images PSP_005043_0930, ESP_013930_0930, ESP_022567_0930, ESP_031837_0930, ESP_041094_0930, ESP_049217_0930, and ESP_058026_0930. Images were acquired between $L_S = 296\text{--}306^\circ$ except for the Mars Year 32 image at $L_S = 317^\circ$. North is up and illumination is from the left in all panels).

sometimes within the same crater (Landis et al., 2021). It is unknown whether the polar cap is gaining or losing mass overall (e.g., Byrne, 2009; I. B. Smith et al., 2020).

Steep scarps in the upper mid-latitudes provide cross sections through H_2O ice deposits (Dundas et al., 2018). These scarps appear to be actively retreating due to sublimation: rocks were observed to fall from one scarp, and several exhibit mottled changes in albedo patterns over the course of the summer, as well as weakening of H_2O spectral features. Sublimation rates are not directly measurable with the present data, but values of one to several mm/Mars year are likely, based on the frequency of falling boulders (Dundas et al., 2018).

5.2. Mass Wasting Processes

Steep, icy cliffs at the edge of the north polar layered deposits (NPLD) exhibit some of the most active mass wasting processes anywhere on Mars. These fall into two categories: avalanches and blockfalls. Avalanches (Figure 12) are so named due to their morphologic similarity to terrestrial “powder snow avalanches” and “dry, loose snow avalanches” (McClung & Schaerer, 2006; Russell et al., 2008). The avalanches occur almost exclusively during early northern spring, between $L_S = 5\text{--}70^\circ$ (Becerra et al., 2020; Russell et al., 2008) and are regularly observed in action by HiRISE. Given that HiRISE observations have a duration of a few seconds, avalanches must occur very frequently. Recent cataloging of avalanches on one especially active marginal scarp implies numerous avalanches per sol during the active season (Becerra et al., 2020). The avalanches often appear as dense clouds of reddish, air-lofted material moving down the steepest sections ($>50^\circ$ slope) of south and southwest-facing NPLD marginal scarps with heavily fractured walls. The avalanche clouds range in extent from just a few tens of meters to more than 200 m. Observations of many avalanche events at different stages allowed a deduction of the course of a typical event: Avalanches start at a discrete point on the steep face and remain small and optically thick as they descend. Upon reaching the basal unit, they spread outward at speeds of several m/s (measured from color fringing in HiRISE images

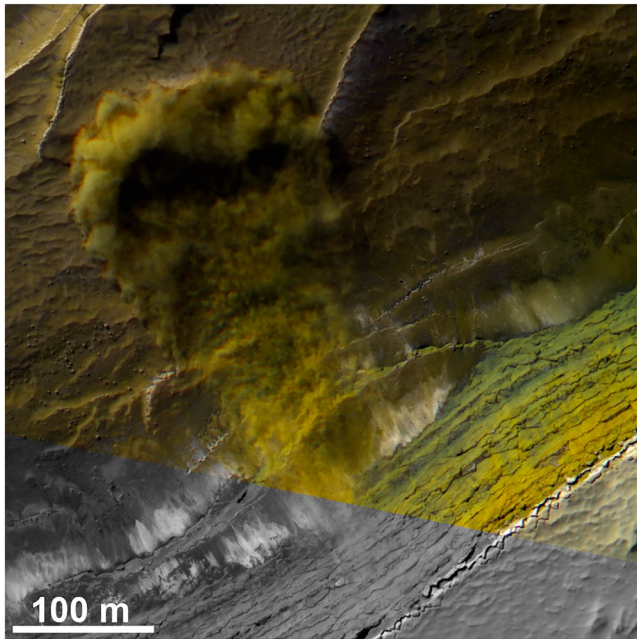


Figure 12. Avalanche cloud at the edge of the north polar layered deposits. Note color fringing near the avalanche toe due to motion of the cloud between acquisition of different colors (Subsection of High Resolution Imaging Science Experiment [HiRISE] image ESP_060176_2640. Color data are only acquired in the central swath of HiRISE images; lower part of the figure is red channel only. North is to the right and illumination is from the top).

[Russell et al., 2008]), become optically thinner, and develop a more diffuse boundary. The avalanches then transition to near-stationary clouds close to, but detached from the scarp, which presumably slowly settle onto the exposed basal unit.

The seasonal occurrence of these avalanches coincides with both the sublimation of seasonal CO₂ ice over the north polar region, and with a peak in subsurface compressional stresses due to solar heating of the scarp walls (Byrne et al., 2017). Thus, there is some debate as to whether the avalanches are triggered directly by subliming CO₂ ice, implying that a significant fraction of the cloud composition would be CO₂ frost, or through fracturing and debris shedding, implying cloud compositions of mostly pulverized water ice and dust (Becerra et al., 2020; Byrne et al., 2017). The earliest HiRISE images taken of these scarps appear to show that, as early as $L_S = 350^\circ$, all CO₂ frost has already sublimed from the steepest walls where the avalanches originate. However, CRISM spectra of the same locations show absorption bands diagnostic of CO₂ until after $L_S = 50^\circ$ (Becerra et al., 2020). Although the CRISM observations support the presence of CO₂ on the walls and in the avalanche clouds, they do not prove that the events are in fact triggered by the sublimating ice.

Russell et al. (2008) also reported two fallen ice blocks at the edge of the NPLD. Subsequent HiRISE observations reveal many more blockfalls (Figure 13) along steep scarps in the NPLD, indicating an estimated slope retreat rate of approximately 0.2 m/kyr (Fanara et al., 2020). Less-common, larger mass-wasting events are also visible (e.g., Figures 13c and 13d). These steep scarps occur only where the underlying dark, basal unit is exposed. Erosion of this sand-rich unit can undercut the more competent, overlying NPLD and cause mass wasting. Local flow of these steep, high-relief icy cliffs could be significant (Sori et al., 2016) but has not been observed. Russell et al. (2014) found that blockfalls from the NPLD occur primarily during late summer through early winter

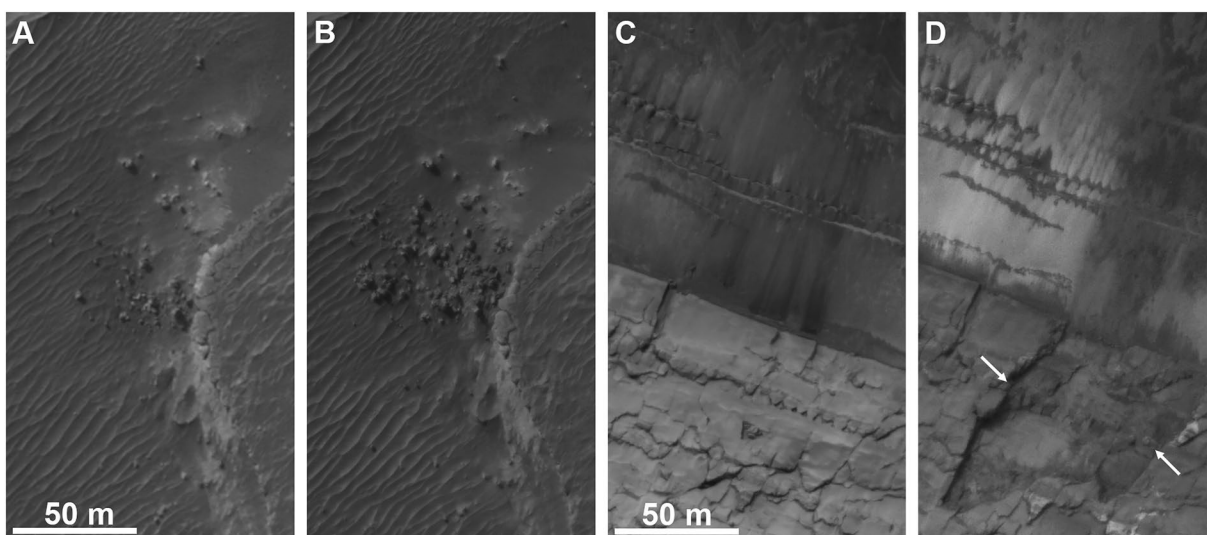


Figure 13. Blockfalls on steep slopes in the north polar layered deposits indicating large morphological changes. (a and b) Blockfall in a small basal scarp, showing fall of a 5×22 m block and new rubble. (c and d) Socket left by fall of a 70 m slab of ice from the face of a steep scarp ((a): Subsection of High Resolution Imaging Science Experiment [HiRISE] image PSP_001628_2650 [Mars Year, MY 28, $L_S = 144^\circ$]. (b): Subsection of HiRISE image ESP_054663_2650 [MY 29, $L_S = 149^\circ$]. (c): Subsection of HiRISE image ESP_016292_2640 (MY 30, $L_S = 39^\circ$). (d): Subsection of HiRISE image ESP_024639_2640 [MY 31, $L_S = 22^\circ$]. North is to the lower right and illumination is from the upper left in all panels).

(likely concentrated before late autumn), while mass wasting on the underlying basal unit favors late summer. Thermoelastic modeling indicates that extensional stresses, which can cause surface-normal fractures, are greatest in winter (Byrne et al., 2017), generally consistent with HiRISE observations, but that compressional stresses, which can cause exfoliation of slabs, occur in the early spring.

6. Tectonic and Volcanic Processes

Tectonic and volcanic processes are both likely to have occurred in geologically recent times, but present-day geomorphic effects have not been convincingly shown. Fault movement is likely active on Mars, given that the InSight lander has reported 174 marsquakes (Giardini et al., 2020). Two of the largest detected marsquakes were located near the Cerberus Fossae fracture system, making these strong candidates for fault motion. Previously, Viking Lander 2 may have detected at least one marsquake, but challenges imposed by the wind, low temporal resolution, and mechanical coupling of the seismometer to the lander made this potential detection ambiguous (Anderson et al., 1977). However, no new offsets on active Martian faults have been observed to date. Seismic acceleration is a possible contributor to all forms of mass wasting, particularly rockfalls (e.g., J. R. Brown & Roberts, 2019; Roberts et al., 2012), but its effects have not yet been determined.

Volcanic eruptions are thought to have occurred on Mars in geologically recent times (e.g., Berman & Hartmann, 2002), but there is no convincing evidence of contemporary activity. Roberts et al. (2007) proposed active volcanic venting in the Cerberus Fossae region. Their argument was based on halos of dark material around small craters and fissures. However, the crater morphology is consistent with impact, and the HiRISE data demonstrate that the craters have bedforms on the floor and are not nearly as deep as suggested, likely because dark sand in the MOC images was interpreted as shadow. Martian wind directions commonly rotate through 360° during the day (e.g., Martínez et al., 2017), so an aeolian explanation involving concentrated sand movement around sand-trapping craters and fissures is likely. An interpretation of recent volcanic activity was recently revived by Horvath et al. (2021) but does not imply the present-day activity. Sori and Bramson (2019) suggested that a local heat anomaly from recent magmatism would be needed to explain putative subsurface water near the south pole (Orosei et al., 2018), but no surface manifestation of such magmatism has been reported.

Putative detections of atmospheric methane in excess of 20 ppbv, including reported spatial and seasonal variability (e.g., Mumma et al., 2009), have led to suggestions of ongoing release of magmatic gases (e.g., Allen et al., 2006). However, the instrument suite of the ExoMars TGO shows extremely low upper limits in the atmosphere, less than 0.06 ppbv above a few km altitude (Knutsen et al., 2021; Korablev et al., 2019). The *Curiosity* rover reports seasonally variable near-surface methane abundances of 0.24–0.65 ppbv in Gale crater following corrections for methane contamination inside the rover (Webster et al., 2018). At present, the explanation of this discrepancy and the implications of atmospheric methane for the current geologic activity remain unresolved. No surface changes attributed to active gas release from the subsurface have been reported.

7. Discussion

7.1. Geologic History of Mars

Mars has been cold and dry, with a low atmospheric pressure, for much of the Amazonian epoch. The modern surface is nevertheless dynamic, with many young features and landforms. Climate and volatile processes are thus key issues for understanding two-thirds of Martian history. How has the Amazonian surface been shaped? How has the climate evolved over that time, and to what extent has it been capable of producing liquid water at the surface? To fully understand the importance of the present-day activity, it is necessary to catalog the suite of current changes, quantify their rates, and to understand the controlling processes and their variation over time. Only then can we learn which landforms indicate the same processes as the present, and which features indicate rare events not yet observed or processes that no longer operate.

Present-day Mars is a dynamic world, with diverse surface changes occurring at all latitudes and seasons (Figures 14 and 15). Over what timescales can lessons from present-day Mars be applied? The answer to this

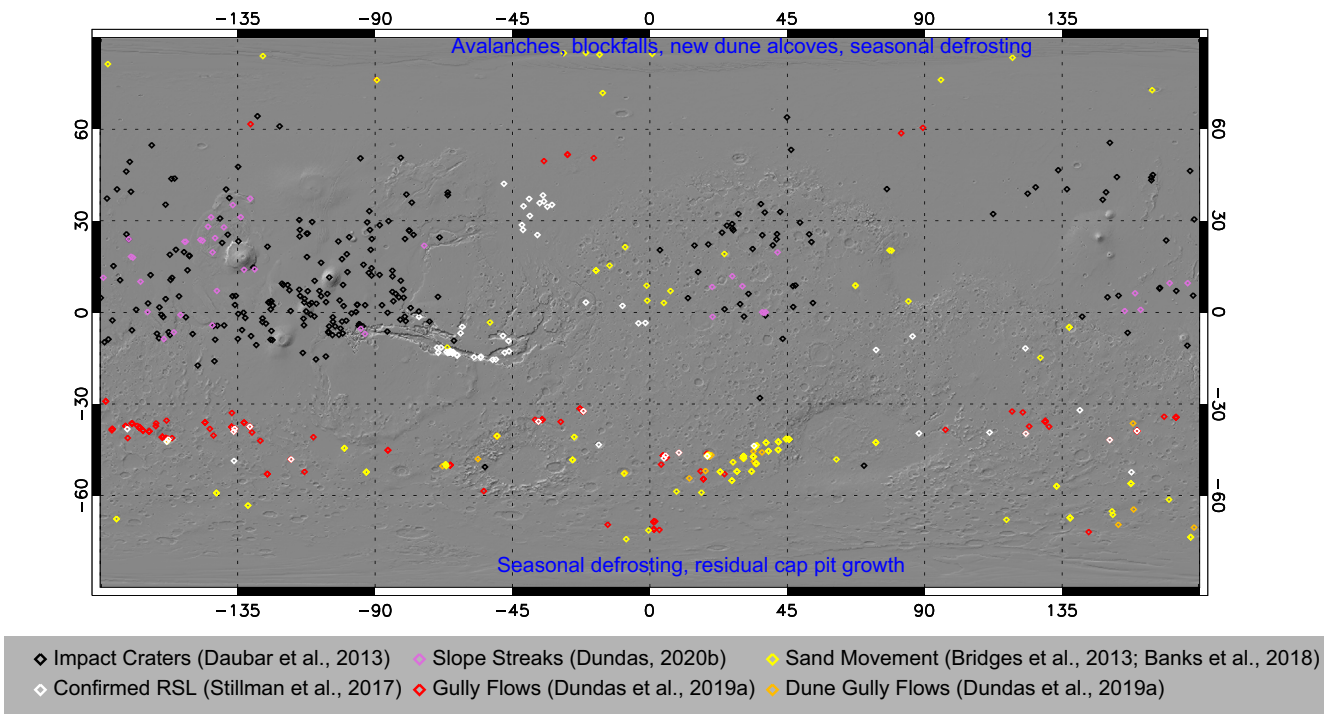


Figure 14. Distributions of surface changes from selected publications. Biases and incompleteness in the distribution of detections may exist due to the nature of the change detection methods and underlying data. Background is shaded relief from Mars Orbiter Laser Altimeter Digital Elevation Model.

question is unfortunately ill-defined at this time: similar geomorphic activity should have been occurring for as long as the climate and surface conditions have been similar. Mars has undergone long-term climate change likely driven primarily by atmospheric loss and sequestration in the crust (e.g., Carr & Head, 2010; Jakosky et al., 2017; Kite et al., 2014; Mahaffy et al., 2015; Scheller et al., 2021). The Noachian and Hesperian epochs had greater aqueous alteration (e.g., Bibring et al., 2006; Ehlmann & Edwards, 2014) and liquid water sufficient to produce lakes and deltas (e.g., Di Achille & Hynek, 2010; Fassett & Head, 2008). Some level of occasional fluvial activity has likely persisted well into the Amazonian (e.g., Grant & Wilson, 2011; Wilson et al., 2016). The ancient climate is still not well understood, but was undoubtedly quite different from the present (e.g., Wordsworth, 2016). Superimposed on this secular trend are cyclic variations resulting from changes in Mars' orbit and obliquity (e.g., Laskar et al., 2004). These variations alter the distribution of insolation, and trap or release significant amounts of CO₂ ice from the polar caps (Bierson et al., 2016; Buhler et al., 2020), potentially doubling (or more) the atmospheric pressure relative to present-day conditions. The key question is which parts of this history required a fundamentally different environment and processes, rather than variations in the intensity and frequency of those processes occurring at present. To address this question, it is necessary to understand the processes underlying the present-day activity and to search the geologic and geomorphic record for features that cannot be explained by modern processes.

Equifinality, the principle that similar morphologies and landforms may result from more than once process, challenges this approach. The best way to resolve questions of equifinality is to observe the formation processes in action, or at minimum to constrain the processes to short time periods in which the environmental conditions are understood. A better understanding of the present-day activity would give us a much-improved ability to interpret the significance of the current surface morphology and a critical lever for interpreting past climate records. Gullies provide an excellent example for how this principle can affect our understanding of Late Amazonian surface processes. Observations point to CO₂ frost processes being the primary driver of the present-day activity and exerting significant control on gully morphology. It remains a key question whether gully formation also involved past liquid water, and the answer remains a high priority because this would place strong requirements on geologically recent climate conditions leading to snowpacks and snowmelt (or alternatively, global hydrology cycles, water abundance, and groundwater

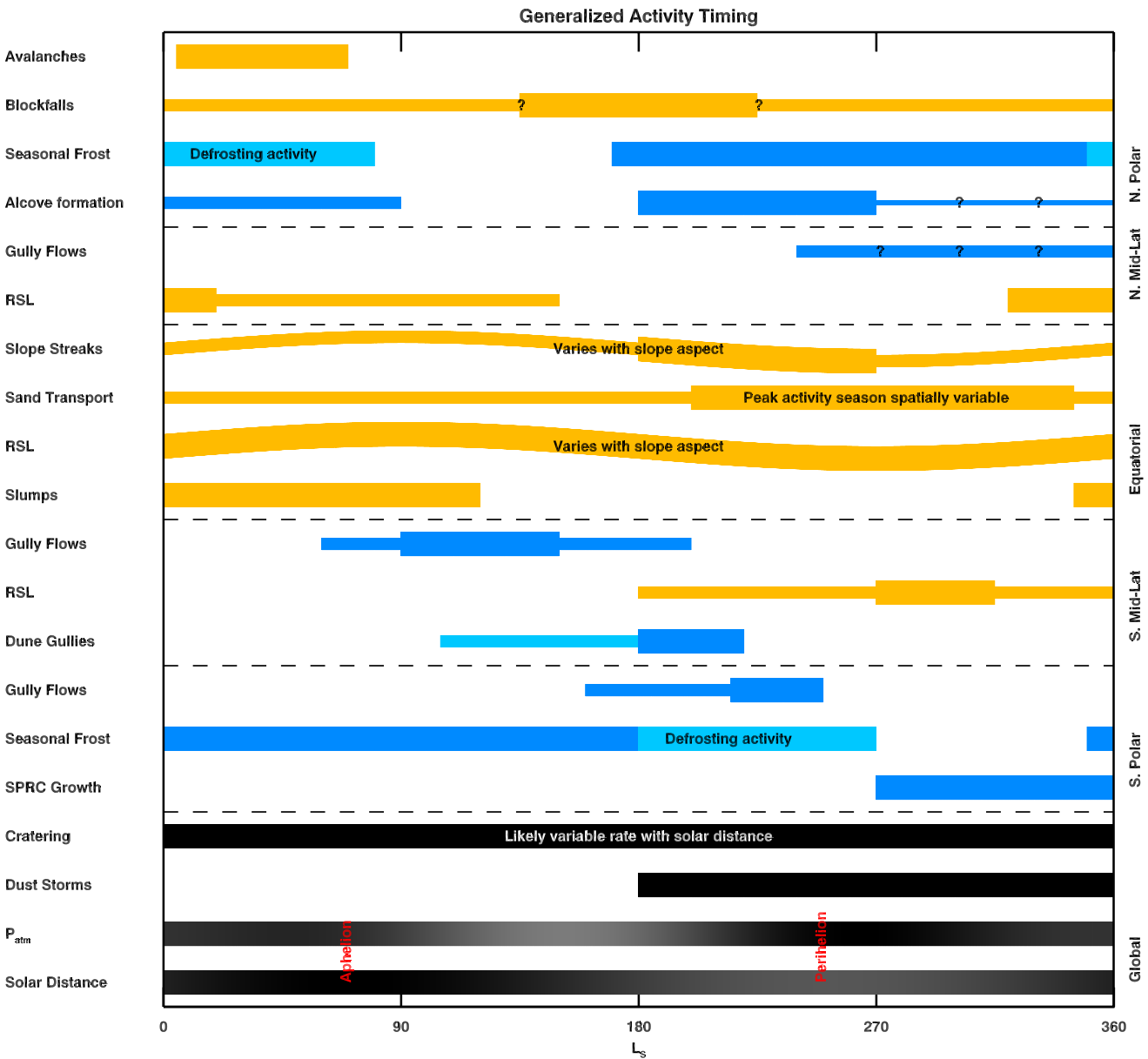


Figure 15. Timing associated with different activity categories. Thick lines indicate primary activity periods; sinuous lines indicate activity that varies seasonally with slope aspect. Lines indicate the general interpreted timing of activity, not the full envelope of uncertainty for all observed events. Some constraints are based on a limited number of sites or examples and could be improved by expanded data. Aeolian sand transport occurs at most latitudes and the seasonality likely varies with latitude and regional wind pattern. Blue lines indicate activity that has been associated with seasonal frost with light blue indicating defrosting activity such as spots and fans; gold lines indicate processes not attributed to frost.

release). Future studies of changing gullies could help differentiate between wet and dry models by better characterizing the scope of morphological changes that can occur in a dry environment. Ultimately, a landed mission may be needed to elucidate many more details about the working of CO₂ frost processes and the landforms that they produce. Landed missions could even potentially determine absolute ages of individual gully deposits via luminescence methods (Cohen et al., 2019) so as to correlate activity rates with Mars' orbital history. With such gains in understanding, we would better be able to extrapolate present-day processes and rates back in time and determine whether they are sufficient to account for observed gully sizes, shapes, and distributions, or whether any observations require past liquid water. A better understanding

of the roles of CO₂ and H₂O in gully formation would provide strong leverage for understanding the climate throughout the timescale of gully formation.

Numerous other examples illustrate the essential connection between learning about modern activity and understanding the entire history of the Amazonian. For instance, the evolution of the south polar residual CO₂ cap may be in a steady state (Byrne, Russell, et al., 2008) or the cap could be in the process of net retreat (Malin et al., 2001). Its state is closely connected to the evolution of the larger CO₂ units in the polar layered deposits (Buhler et al., 2020), so the evolving south polar residual cap is a critical piece of Mars' recent climate history. Learning, which aeolian bedforms are currently active and inactive, and when and why the latter was active in the past, is likewise fundamental to understanding recent atmospheric pressure changes and wind patterns.

Understanding how current processes shape geomorphology would also be important for interpreting other climate records. Historical records of climate signals from the Late Amazonian likely exist in ice deposits (e.g., I. B. Smith et al., 2018); likewise, these deposits contain information on how the efficiency of dust-lifting varies with orbital elements, and the mobility of dust is key to many of the surface changes discussed herein. Effectively interpreting signals within polar or mid-latitude ice requires the ability to link measurable variables in the ice to past climate conditions across the planet. Geomorphology can provide one avenue to do this: determining the ages and formation processes of landforms constrains the climate during and after formation.

As our understanding of uniquely Martian present-day processes develops, it is of great interest to apply these lessons toward studies of ancient Mars. Modern Martian activity has proven surprising in several ways, causing us to question repeatedly the extension of terrestrial (and often water-based) process models. This raises the possibility that interpretations of ancient conditions are incomplete because they have not considered how the full suite of contemporary processes might have operated in the past, and/or because yet more uniquely Martian processes remain to be discovered. As one example, seasonal CO₂ frost is also predicted in climate models with a denser past atmosphere (e.g., Forget et al., 2013), but the possible consequences of this (such as the formation of ancient araneiforms or gully flow-like processes) have not yet been investigated.

Recent studies have shown that modern processes alone are sufficient to create or reshape many of the surface features discussed in this paper. However, it is also true that much of Mars' surface is ancient, with very low average resurfacing or erosion rates (e.g., Golombek et al., 2006). These observations can be reconciled by recognizing that much of the present-day activity (and presumably similar activity over several billion years) is superficial, or primarily affects only certain substrates. In particular, volatile-rich deposits (CO₂ and H₂O ices) and aeolian-transportable materials (sand and dust) are particularly susceptible to modification by a range of processes and are likely eroded and deposited on short timescales. Other processes are confined to steep slopes and thus are naturally self-limiting. These limitations enable present-day processes to shape and rework much of the fine-scale geomorphology, while the older material dominates the topography at large scales.

7.2. Open Questions Regarding Present-Day Activity

Landed missions and very high-resolution orbital imaging (HiRISE) have been required to definitively detect and characterize many of the currently known active processes on Mars. Consequently, the record of present-day Martian surface changes is highly incomplete due to very limited areal coverage and is subject to observational biases. Broader monitoring campaigns may yet detect new active processes and styles of change and reveal spatial variations in the nature of those currently known. Longer temporal coverage and/or monitoring from the surface would likely reveal additional types of activity in addition to expanding the record of known processes. Moreover, the long-term rates of topographic change and mass fluxes of most processes are poorly known, since many changes are not resolved by HiRISE digital terrain models. Without this information, it is challenging to quantify the long-term effects of the present-day activity or understand how it changes over time, even if it is geomorphically significant under modern conditions.

This overview has focused on changes that are observed from orbit, or within the tiny fraction of the surface explored by landed missions. It is important to recognize that there are likely other types of change that are actively shaping present-day Mars but that have not yet been detected because observations of the appropriate spatial or temporal scale have not been acquired. Two such examples of likely but unobserved activity are thermal contraction cracking in subsurface ice and the geomorphic effects of H₂O sublimation. Models predict that thermal contraction cracking should occur in the modern Martian climate, but with centimeter-scale effects that would require thousands of years to change the surface at scales observable from orbit (Mellon et al., 2008). The Phoenix lander observed furrows in regolith and cracks in the ice that suggest that this process is active (Mellon et al., 2009), but the spacecraft did not operate long enough to document changes. A few similar troughs, without the sharper cracks, were observed by Viking Lander 2 (Mutch et al., 1977). Evolution of scalloped depressions via sublimation may also be active but too slow to be detected (Dundas, Byrne, & McEwen, 2015), as may also be the case for flow of debris-covered mid-latitude glaciers (Sori et al., 2017). H₂O ice sublimation is likely occurring in many places but from orbit can only be observed where it results in rockfalls from icy slopes (Dundas et al., 2018).

Understanding of the processes driving many forms of modern Martian activity is incomplete. Developing such understanding through theory and experiments is necessary to improve predictions and interpretations. Terrestrial analogs are useful but limited, and dry, volatile-free processes on Mars are operating under conditions that have less water than even the driest environments on Earth. In many cases, in situ studies by landed missions may be required to identify and understand the processes at work. Several critical areas stand out as needing improved understanding: the variety of processes caused by CO₂ frost and the behavior of dry granular flows under Martian conditions. These two may overlap in understanding gully formation. The former is important because CO₂ frost is widespread, appears to be a major geomorphic agent, and is poorly analogous to anything on present-day Earth. Such Martian processes could serve as an analog to landscape evolution on other worlds with volatile ice deposits such as Io, Triton, and Pluto. The latter is relevant because dry (or CO₂-mediated) flows appear to occur in several different ways on Mars, in a variety of settings and substrates. Better knowledge of how these occur and are differentiated would greatly improve understanding of modern Martian systems and enable better discrimination between such flows and those that may have been fluidized by water. Additionally, more information is needed regarding the behavior and properties of Martian dust. Dust lifting is not fully understood (e.g., Neakrase et al., 2016), but is a fundamental driver of both surface change and climate. Furthermore, many active surface features occur within dust, but may be brighter or darker than the undisturbed surface and persist for widely varying amounts of time.

Several more specific questions can be identified for each of the categories of change discussed above. While a complete list would be long, several key issues are highlighted here:

1. For impact cratering, what is the true slope of the observed small-crater production function and how does it transition to the slope at larger diameters? How representative of the long-term average is the current impact flux, and how does it vary seasonally? The seasonal variation due to different solar distance should also map directly to the effects of long-term variations of the eccentricity of Mars' orbit.
2. For aeolian processes, what affects surface transport and lifting of dust, a fundamental control on atmospheric physics? Which bedforms are inactive in the present climate, and what determines when they are active?
3. For slope processes, do gullies form entirely via CO₂ processes, or were aqueous processes involved in the past? For RSL and slope streaks, most recent evidence points to dry rather than wet flow processes, but how do such granular flows work in detail, and is it possible to definitively demonstrate or rule out present-day liquid water?
4. For polar and seasonal-frost processes, our understanding of the "Kieffer model" (Kieffer, 2007) and related processes is largely based on models and small-scale laboratory experiments, due to a lack of terrestrial analogs. Hypotheses based only on theory and orbital data may be missing important components. Additionally, a fundamental question remains open: are the southern CO₂ and northern H₂O residual caps currently gaining or losing mass? This is a fundamental calibration point for understanding Mars' energy budget, global volatile transport, and the effects of varying orbital and climate conditions.

Potentially, morphological effects of evolution of the buried south polar CO₂ deposits could be observed if they are interacting with the atmosphere.

Answering these questions would fundamentally improve our knowledge of how Martian processes work at present, and thus how Mars has changed over time. These answers also help guide decisions about defining special regions for enhanced levels of planetary protection (Rummel et al., 2014).

8. Conclusions

The surface of Mars is being actively shaped by many processes. Several of these were not predicted a priori and have no terrestrial analog. This diverse suite of changes affects the entire planet, but most strongly influence aeolian-transported or volatile-rich materials that form a mobile veneer on older surface materials. Understanding this type of activity is necessary to accurately interpret climate variations throughout the Amazonian: without understanding present-day processes, it is not possible to determine how they have varied over time, what influence they have had on the past and present surface of Mars, and how they affect our ability to interpret ancient Mars.

Data Availability Statement

HiRISE and CTX data are available via the Planetary Data System Imaging Node at <https://pds-imaging.jpl.nasa.gov/volumes/mro.html> (<https://doi.org/10.17189/1520303> and <https://doi.org/10.17189/1520266>) and MOC data are available at <https://pds-imaging.jpl.nasa.gov/volumes/mgs.html> (<https://doi.org/10.17189/1520255>). Map-projected HiRISE images courtesy NASA/JPL/University of Arizona. CaSSIS raw data are available via ESA's Planetary Science Archive at <https://archives.esac.esa.int/psa/#!Table%20View/CaSSIS=instrument>. Fully processed data, as well as color browse products are available at <http://cassiss.halimed.unibe.ch/observations>. MOLA data used in Figure 14 are available at <https://pds-geosciences.wustl.edu/missions/mgs/megdr.html> (<https://doi.org/10.17189/1519460>) and feature data are in the cited references.

References

- Abotalib, A. Z., & Heggy, E. (2019). A deep groundwater origin for recurring slope lineae on Mars. *Nature Geoscience*, *12*, 235–241. <https://doi.org/10.1038/s41561-019-0327-5>
- Aharonson, O. (2007). *The modern impact cratering flux at the surface of Mars*. Lunar and Planetary Science Conference 38, abstract #2288.
- Aharonson, O., Schorghofer, N., & Gerstell, M. F. (2003). Slope streak formation and dust deposition rates on Mars. *Journal of Geophysical Research*, *108*, 5138. <https://doi.org/10.1029/2003JE002123>
- Allen, M., Sherwood Lollar, B., Runnegar, B., Oehler, D. Z., Lyons, J. R., Manning, C. E., & Summers, M. E. (2006). Is Mars alive? *Eos, Transactions, American Geophysical Union*, *87*, 433–439. <https://doi.org/10.1029/2006EO410001>
- Amador, E. S., Mushkin, A., & Gillespie, A. (2016). *Spectral characteristics of dark slope streaks on Mars: A global survey with CRISM*. Lunar and Planetary Science Conference 47, abstract #2696. <https://doi.org/10.1002/chin.201613261>
- Anderson, D. L., Miller, W. F., Latham, G. V., Nakamura, Y., Toksöz, M. N., Dainty, A. M., et al. (1977). Seismology on Mars. *Journal of Geophysical Research*, *82*, 4524–4546. <https://doi.org/10.1029/J082i028p04524>
- Arvidson, R. E., Guinness, E. A., Moore, H. J., Tillman, J., & Wall, S. D. (1983). Three Mars years: Viking Lander 1 imaging observations. *Science*, *222*, 463–468. <https://doi.org/10.1126/science.222.4623.463>
- Ayoub, F., Avouac, J.-P., Newman, C. E., Richardson, M. I., Lucas, A., Leprince, S., & Bridges, N. T. (2014). Threshold for sand mobility on Mars calibrated from seasonal variations of sand flux. *Nature Communications*, *5*, 5096. <https://doi.org/10.1038/ncomms6096>
- Baker, M. M., Lapotre, M. G. A., Miniti, M. E., Newman, C. E., Sullivan, R., Weitz, C. M., et al. (2018). The Bagnold Dunes in southern summer: Active sediment transport on Mars observed by the Curiosity rover. *Geophysical Research Letters*, *45*, 8853–8863. <https://doi.org/10.1029/2018GL079040>
- Balme, M., Berman, D. C., Bourke, M. C., & Zimbelman, J. R. (2008). Transverse Aeolian Ridges (TARs) on Mars. *Geomorphology*, *101*, 703–720. <https://doi.org/10.1016/j.geomorph.2008.03.011>
- Banfield, D., Spiga, A., Newman, C., Forget, F., Lemmon, M., Lorenz, R., et al. (2020). The atmosphere of Mars as observed by InSight. *Nature Geoscience*, *13*, 190–198. <https://doi.org/10.1038/s41561-020-0534-0>
- Banks, M. E., Fenton, L. K., Bridges, N. T., Geissler, P. E., Chojnacki, M., Runyon, K. D., et al. (2018). Patterns in mobility and modification of middle- and high-latitude southern hemisphere dunes on Mars. *Journal of Geophysical Research: Planets*, *123*, 3205–3219. <https://doi.org/10.1029/2018JE005747>
- Baratoux, D., Mangold, N., Forget, F., Cord, A., Pinet, P., Daydou, Y., et al. (2006). The role of wind-transported dust in slope streaks activity: Evidence from the HRSC data. *Icarus*, *183*, 30–45. <https://doi.org/10.1016/j.icarus.2006.01.023>
- Bart, G. D., Daubar, I. J., Ivanov, B. A., Dundas, C. M., & McEwen, A. S. (2019). Dark halos produced by current impact cratering on Mars. *Icarus*, *328*, 45–57. <https://doi.org/10.1016/j.icarus.2019.03.004>
- Becerra, P., Byrne, S., & Brown, A. J. (2015). Transient bright “halos” on the South Polar Residual Cap of Mars: Implications for mass balance. *Icarus*, *251*, 211–225. <https://doi.org/10.1016/j.icarus.2014.04.050>

Acknowledgments

CaSSIS is a project of the University of Bern and funded through the Swiss Space Office via ESA's PRODEX program. The instrument hardware development was supported by the Italian Space Agency (ASI), INAF/Astronomical Observatory of Padova, and the Space Research Center (CBK) in Warsaw, as well as by SGF (Budapest), the University of Arizona, and NASA. Colin M. Dundas was funded by a NASA-USGS Interagency Agreement. Patricio Becerra and Adomas Valentinas were funded by Swiss National Science Foundation (SNF) grant 200020_178847. Ingrid J. Daubar was supported by NASA Solar System Workings grant 80NSSC20K0789. Serina Diniega work was carried out at the Jet Propulsion Laboratory, California Institute of Technology, under a contract with the National Aeronautics and Space Administration (80NM0018D0004). Matthew Chojnacki was supported in part by NASA Mars Data Analysis Program grants 80NSSC21K0040 and 80NSSC20K1066. The authors thank the science, operations, and engineering teams of all the spacecraft and instruments that have conducted monitoring studies of the Martian surface, in many cases operating far beyond their design lifetime and enabling studies over long temporal baselines. Mikhail Kreslavsky, Cynthia Dinwiddie, and David Stillman provided detailed and helpful reviews.

- Becerra, P., Herny, C., Valantinas, A., Byrne, S., Thomas, N., & Conway, S. (2020). *Avalanches of the Martian north polar cap*. Europlanet Science Congress 14, abstract #EPSC2020-1093.
- Bergonio, J. R., Rottas, K. M., & Schorghofer, N. (2013). Properties of Martian slope streak populations. *Icarus*, 225, 194–199. <https://doi.org/10.1016/j.icarus.2013.03.023>
- Berman, D. C., Balme, M. R., Rafkin, S. C. R., & Zimbleman, J. (2011). Transverse Aeolian Ridges (TARs) on Mars II: Distribution, orientations, and ages. *Icarus*, 213, 116–130. <https://doi.org/10.1016/j.icarus.2011.02.014>
- Berman, D. C., & Hartmann, W. K. (2002). Recent fluvial, volcanic, and tectonic activity on the Cerberus plains of Mars. *Icarus*, 159, 1–17. <https://doi.org/10.1006/icar.2002.6920>
- Bhardwaj, A., Sam, L., Martín-Torres, F. J., & Zorzano, M.-P. (2019). Are slope streaks indicative of global-scale aqueous processes on contemporary Mars? *Reviews of Geophysics*, 57, 48–77. <https://doi.org/10.1029/2018RG000617>
- Bhardwaj, A., Sam, L., Martín-Torres, F. J., Zorzano, M.-P., & Fonseca, R. M. (2017). Martian slope streaks as plausible indicators of transient water activity. *Scientific Reports*, 7, 7074. <https://doi.org/10.1038/s41598-017-07453-9>
- Bibring, J.-P., Langevin, Y., Mustard, J. F., Poulet, F., Arvidson, R. E., Gendrin, A., et al. (2006). Global mineralogical and aqueous Mars history derived from OMEGA/Mars Express data. *Science*, 312, 400–404. <https://doi.org/10.1126/science.1122659>
- Bibring, J.-P., Langevin, Y., Poulet, F., Gendrin, A., Gondet, B., Berthé, M., et al. (2004). OMEGA team Perennial water ice identified in the south polar cap of Mars. *Nature*, 428, 627–630. <https://doi.org/10.1038/nature02461>
- Bierson, C. J., Phillips, R. J., Smith, I. B., Wood, S. E., Putzig, N. E., Nunes, D., & Byrne, S. (2016). Stratigraphy and evolution of the buried CO₂ deposit in the Martian south polar cap. *Geophysical Research Letters*, 43, 4172–4179. <https://doi.org/10.1002/2016gl068457>
- Bourke, M. C. (2013). *The formation of sand furrows by cryo-venting on Martian dunes*. Lunar and Planetary Science Conference 44, abstract #2919. <https://doi.org/10.1080/03068374.2012.760792>
- Bourke, M. C., Edgett, K. S., & Cantor, B. A. (2008). Recent aeolian dune change on Mars. *Geomorphology*, 94, 247–255. <https://doi.org/10.1016/j.geomorph.2007.05.012>
- Bridges, N. T., Ayoub, F., Avouac, J.-P., Leprince, A., & Mattson, S. (2012). Earth-like sand fluxes on Mars. *Nature*, 485, 339–342. <https://doi.org/10.1038/nature11022>
- Bridges, N. T., Bourke, M. C., Geissler, P. E., Banks, M. E., Colon, C., Diniega, S., et al. (2012). Planet-wide sand motion on Mars. *Geology*, 40, 31–34. <https://doi.org/10.1130/G32373.1>
- Bridges, N. T., Geissler, P., Silvestro, S., & Banks, M. (2013). Bedform migration on Mars: Current results and future plans. *Aeolian Research*, 9, 133–151. <https://doi.org/10.1016/j.aeolia.2013.02.004>
- Bridges, N. T., Geissler, P. E., McEwen, A. S., Thomson, B. J., Chuang, F. C., Herkenhoff, K. E., et al. (2007). Windy Mars: A dynamic planet as seen by the HiRISE camera. *Geophysical Research Letters*, 34, L23205. <https://doi.org/10.1029/2007GL031445>
- Bridges, N. T., Sullivan, R., Newman, C. E., Navarro, S., van Beek, J., Ewing, R. C., et al. (2017). Martian aeolian activity at the Bag-nold Dunes, Gale crater: The view from the surface and orbit. *Journal of Geophysical Research: Planets*, 122, 2077–2110. <https://doi.org/10.1002/2017JE005263>
- Brown, A. J., Calvin, W. M., Becerra, P., & Byrne, S. (2016). Martian north polar cap summer water cycle. *Icarus*, 277, 401–415. <https://doi.org/10.1016/j.icarus.2016.05.007>
- Brown, J. R., & Roberts, G. P. (2019). Possible evidence for variation in magnitude for marsquakes from fallen boulder populations, Grjota Valles, Mars. *Journal of Geophysical Research: Planets*, 124, 801–822. <https://doi.org/10.1029/2018JE005622>
- Brusnikin, E. S., Kreslavsky, M. A., Zubarev, A. E., Patraty, V. D., Krasilnikov, S. S., Head, J. W., & Karachevtseva, I. P. (2016). Topographic measurements of slope streaks on Mars. *Icarus*, 278, 52–61. <https://doi.org/10.1016/j.icarus.2016.06.005>
- Buhler, P. B., Ingersoll, A. P., Piqueux, S., Ehlmann, B. L., & Hayne, P. O. (2020). Coevolution of Mars's atmosphere and massive south polar CO₂ deposit. *Nature Astronomy*, 4, 364–371. <https://doi.org/10.1038/s41550-019-0976-8>
- Byrne, S. (2009). The polar deposits of Mars. *Annual Review of Earth and Planetary Sciences*, 37, 535–560. <https://doi.org/10.1146/annurev.earth.031208.100101>
- Byrne, S., Dundas, C. M., Kennedy, M. R., Mellon, M. T., McEwen, A. S., Cull, S. C., et al. (2009). Distribution of mid-latitude ground ice on Mars from new impact craters. *Science*, 325, 1674–1676. <https://doi.org/10.1126/science.1175307>
- Byrne, S., & Ingersoll, A. P. (2003). A sublimation model for Martian south polar ice features. *Science*, 299, 1051–1053. <https://doi.org/10.1126/science.1080148>
- Byrne, S., Russell, P. S., Fishbaugh, K. E., Hansen, C. J., Herkenhoff, K. E., McEwen, A. S., & HiRISE Team. (2008). *Explaining the persistence of the southern residual cap of Mars: HiRISE data and landscape evolution models*. Lunar and Planetary Science Conference 39, abstract #2252.
- Byrne, S., Sori, M. M., Russell, P., Pathare, A. V., Becerra, P., Molaro, J. L., et al. (2017). *Mars polar cliffs: Stressed out and falling apart*. European Planetary Science Congress, abstract EPSC2017-333.
- Byrne, S., Zuber, M. T., & Neumann, G. A. (2008). Interannual and seasonal behavior of Martian residual ice-cap albedo. *Planetary and Space Science*, 56, 194–211. <https://doi.org/10.1016/j.pss.2006.03.018>
- Calvin, W. M., James, P. B., Cantor, B. A., & Dixon, E. M. (2015). Interannual and seasonal changes in the north polar ice deposits of Mars: Observations from MY 29–31 using MARCI. *Icarus*, 251, 181–190. <https://doi.org/10.1016/j.icarus.2014.08.026>
- Cantor, B. A., Kanak, K. M., & Edgett, K. S. (2006). Mars Orbiter Camera observations of Martian dust devils and their tracks (September 1997 to January 2006) and evaluation of theoretical vortex models. *Journal of Geophysical Research*, 111, E12002. <https://doi.org/10.1029/2006JE002700>
- Carr, M. H., & Head, J. W. (2010). Geologic history of Mars. *Earth and Planetary Science Letters*, 294, 185–203. <https://doi.org/10.1016/j.epsl.2009.06.042>
- Choi, D. S., & Dundas, C. M. (2011). Measurements of Martian dust devil winds with HiRISE. *Geophysical Research Letters*, 38, L24206. <https://doi.org/10.1029/2011GL049806>
- Chojnacki, M., Banks, M. E., Fenton, L. K., & Urso, A. C. (2019). Boundary condition controls on the high-sand-flux regions of Mars. *Geology*, 47, 427–430. <https://doi.org/10.1130/G45793.1>
- Chojnacki, M., Burr, D. M., Moersch, J. E., & Michaels, T. I. (2011). Orbital observations of contemporary dune activity in Endeavour crater, Meridiani Planum, Mars. *Journal of Geophysical Research*, 116, E00F19. <https://doi.org/10.1029/2010JE003675>
- Chojnacki, M., Fenton, L. K., Weintraub, A. R., Edgar, L. A., Jodhpurkar, M. J., & Edwards, C. S. (2020). Ancient martian aeolian sand dune deposits recorded in the stratigraphy of valles marineris and implications for past climates. *Journal of Geophysical Research: Planets*, 125. <https://doi.org/10.1029/2020JE006510>

- Chojnacki, M., Johnson, J. R., Moersch, J. E., Fenton, L. K., Michaels, T. I., & Bell, J. F. (2015). Persistent aeolian activity at Endeavour crater, Meridiani Planum, Mars: New observations from orbit and the surface. *Icarus*, *251*, 275–290. <https://doi.org/10.1016/j.icarus.2014.04.044>
- Chojnacki, M., McEwen, A., Dundas, C., Ojha, L., Urso, A., & Sutton, S. (2016). Geologic context of recurring slope lineae in Melas and Coprates Chasmata, Mars. *Journal of Geophysical Research: Planets*, *121*, 1204–1231. <https://doi.org/10.1002/2015JE004991>
- Chojnacki, M., Urso, A., Fenton, L. K., & Michaels, T. I. (2017). Aeolian dune sediment flux heterogeneity in Meridiani Planum, Mars. *Aeolian Research*, *26*, 73–88. <https://doi.org/10.1016/j.aeolia.2016.07.004>
- Christensen, P. R. (2003). Formation of recent Martian gullies through melting of extensive water-rich snow deposits. *Nature*, *422*, 45–48. <https://doi.org/10.1038/nature01436>
- Christensen, P. R., Jakosky, B. M., Kieffer, H. H., Malin, M. C., McSween, H. Y., Jr., Neelson, K., et al. (2004). The Thermal Emission Imaging System (THEMIS) for the Mars 2001 Odyssey mission. *Space Science Reviews*, *110*, 85–130. <https://doi.org/10.1023/B:SPAC.0000021008.16305.94>
- Chuang, F. C., Beyer, R. A., & Bridges, N. T. (2010). Modification of Martian slope streaks by eolian processes. *Icarus*, *205*, 154–164. <https://doi.org/10.1016/j.icarus.2009.07.035>
- Chuang, F. C., Beyer, R. A., McEwen, A. S., & Thomson, B. J. (2007). HiRISE observations of slope streaks on Mars. *Geophysical Research Letters*, *34*, L20204. <https://doi.org/10.1029/2007GL031111>
- Clancy, R. T., Sandor, B. J., Wolff, M. J., Christensen, P. R., Smith, M. D., Pearl, J. C., et al. (2000). An intercomparison of groundbased millimeter, MGS TES, and Viking atmospheric temperature measurements: Seasonal and interannual variability of temperatures and dust loading in the global Mars atmosphere. *Journal of Geophysical Research*, *105*, 9553–9571. <https://doi.org/10.1029/1999JE001089>
- Cohen, B. A., Malespin, C. A., Farley, K. A., Martin, P. E., Cho, Y., & Mahaffy, P. R. (2019). In Situ geochronology on Mars and the development of future instrumentation. *Astrobiology*, *19*, 1303–1314. <https://doi.org/10.1089/ast.2018.1871>
- Conway, S. J., & Balme, M. R. (2014). Decimeter thick remnant glacial ice deposits on Mars. *Geophysical Research Letters*, *41*, 5402–5409. <https://doi.org/10.1002/2014GL060314>
- Conway, S. J., de Haas, T., & Harrison, T. N. (2019). Martian gullies: A comprehensive review of observations, mechanisms and insights from Earth analogues. *Geological Society, London, Special Publications*, *467*, 7–66. <https://doi.org/10.1144/SP467.14>
- Cushing, G. E., Titus, T. N., & Christensen, P. R. (2005). THEMIS VIS and IR observations of a high-altitude Martian dust devil. *Geophysical Research Letters*, *32*, L23202. <https://doi.org/10.1029/2005GL024478>
- Daubar, I. J., Banks, M. E., Scharrer, N. C., & Golombek, M. P. (2019). Recently formed crater clusters on Mars. *Journal of Geophysical Research: Planets*, *124*, 958–969. <https://doi.org/10.1029/2018JE005857>
- Daubar, I. J., Dundas, C. M., Byrne, S., Geissler, P., Bart, G. D., McEwen, A. S., et al. (2016). Changes in blast zone albedo patterns around new Martian impact craters. *Icarus*, *267*, 86–105. <https://doi.org/10.1016/j.icarus.2015.11.032>
- Daubar, I. J., Gao, A., Wexler, D., Dundas, C., McEwen, A., Neidhart, T., et al. (2020). *New craters on Mars: An updated catalog*. 11th Planetary Crater Consortium, abstract #2069.
- Daubar, I. J., McEwen, A. S., Byrne, S., & Kennedy, M. R. (2012). *Seasonal variation in current Martian impact rate*. Lunar and Planetary Science Conference 43, abstract #2740.
- Daubar, I. J., McEwen, A. S., Byrne, S., Kennedy, M. R., & Ivanov, B. (2013). The current Martian cratering rate. *Icarus*, *225*, 506–516. <https://doi.org/10.1016/j.icarus.2013.04.009>
- Daubar, I. J., Ojha, L., Chojnacki, M., Golombek, M., Lorenz, R., Wray, J., & Lewis, K. (2018). *Lifetime of a dust devil track and dust deposition rate in Gusev crater*. Lunar and Planetary Science Conference 49, abstract #1730.
- Day, M., & Dorn, T. (2019). Wind in Jezero crater, Mars. *Geophysical Research Letters*, *46*, 3099–3107. <https://doi.org/10.1029/2019GL082218>
- Day, M., & Rebolledo, L. (2019). Intermittency in wind-driven surface alteration on Mars interpreted from wind streaks and measurements by InSight. *Geophysical Research Letters*, *46*, 12747–12755. <https://doi.org/10.1029/2019GL085178>
- de Haas, T., McARDell, B. W., Conway, S. J., McElwaine, J. N., Kleinhans, M. G., Salese, F., & Grindrod, P. M. (2019). Initiation and flow conditions of contemporary flows in Martian gullies. *Journal of Geophysical Research: Planets*, *124*, 2246–2271. <https://doi.org/10.1029/2018JE005899>
- Delamere, W. A., Tornabene, L. L., McEwen, A. S., Becker, K., Bergstrom, J. W., Bridges, N. T., et al. (2010). Color imaging of Mars by the High Resolution Imaging Science Experiment (HiRISE). *Icarus*, *205*, 38–52. <https://doi.org/10.1016/j.icarus.2009.03.012>
- Di Achille, G., & Hynes, B. M. (2010). Ancient global ocean on Mars supported by global distribution of deltas and valleys. *Nature Geoscience*, *3*, 459–463. <https://doi.org/10.1038/NGEO891>
- Dickson, J. L., Head, J. W., & Kulowski, M. (2016). *Active flows at the Mars Science Laboratory landing site: Results from a survey of Mastcam imagery through Sol 971*. Lunar and Planetary Science Conference 47, abstract #1726. <https://doi.org/10.1002/chin.201621190>
- Diniega, S., Bramson, A. M., Buratti, B., Buhler, P., Burr, D. M., Chojnacki, M., et al. (2021). Modern Mars' geomorphological activity, driven by wind, frost, and gravity. *Geomorphology*, *380*, 107627. <https://doi.org/10.1016/j.geomorph.2021.107627>
- Diniega, S., Byrne, S., Bridges, N. T., Dundas, C. M., & McEwen, A. S. (2010). Seasonality of present-day Martian dune-gully activity. *Geology*, *38*, 1047–1050. <https://doi.org/10.1130/G31287.1>
- Diniega, S., Hansen, C. J., Allen, A., Grigsby, N., Li, Z., Perez, T., & Chojnacki, M. (2019). Dune-slope activity due to frost and wind throughout the north polar erg, Mars. *Geological Society, London, Special Publications*, *467*, 95–114. <https://doi.org/10.1144/SP467.5610.1144/sp467.6>
- Diniega, S., Hansen, C. J., McElwaine, J. N., Hugenholtz, C. H., Dundas, C. M., McEwen, A. S., & Bourke, M. C. (2013). A new dry hypothesis for the formation of Martian linear gullies. *Icarus*, *225*, 526–537. <https://doi.org/10.1016/j.icarus.2013.04.006>
- Diniega, S., Kreslavsky, M., Radebaugh, J., Silvestro, S., Telfer, M., & Tirsch, D. (2017). Our evolving understanding of aeolian bedforms, based on observations of dunes on different worlds. *Aeolian Research*, *26*, 5–27. <https://doi.org/10.1016/j.aeolia.2016.10.001>
- Dinwiddie, C. L., & Titus, T. N. (2021). Airborne dust plumes lofted by dislodged ice blocks at Russell crater, Mars. *Geophysical Research Letters*, *48*, e2020GL091920. <https://doi.org/10.1029/2020GL091920>
- Dundas, C. M. (2020a). An aeolian grainflow model for Martian recurring slope lineae. *Icarus*, *343*, 113681. <https://doi.org/10.1016/j.icarus.2020.113681>
- Dundas, C. M. (2020b). Geomorphological evidence for a dry dust avalanche origin of slope streaks on Mars. *Nature Geoscience*, *13*, 473–476. <https://doi.org/10.1038/s41561-020-0598-x>
- Dundas, C. M., Bramson, A. M., Ojha, L., Wray, J. J., Mellon, M. T., Byrne, S., et al. (2018). Exposed subsurface ice sheets in the Martian mid-latitudes. *Science*, *359*, 199–201. <https://doi.org/10.1126/science.aao1619>
- Dundas, C. M., & Byrne, S. (2010). Modeling sublimation of ice exposed by new impacts in the Martian mid-latitudes. *Icarus*, *206*, 716–728. <https://doi.org/10.1016/j.icarus.2009.09.007>

- Dundas, C. M., Byrne, S., & McEwen, A. S. (2015). Modeling the development of Martian sublimation thermokarst landforms. *Icarus*, 262, 154–169. <https://doi.org/10.1016/j.icarus.2015.07.033>
- Dundas, C. M., Byrne, S., McEwen, A. S., Mellon, M. T., Kennedy, M. R., Daubar, I. J., & Saper, L. (2014). HiRISE observations of new impact craters exposing Martian ground ice. *Journal of Geophysical Research: Planets*, 119, 109–127. <https://doi.org/10.1002/2013JE004482>
- Dundas, C. M., Diniega, S., Hansen, C. J., Byrne, S., & McEwen, A. S. (2012). Seasonal activity and morphological changes in Martian gullies. *Icarus*, 220, 124–143. <https://doi.org/10.1016/j.icarus.2012.04.005>
- Dundas, C. M., Diniega, S., & McEwen, A. S. (2015). Long-term monitoring of Martian gully formation and evolution with MRO/HiRISE. *Icarus*, 251, 244–263. <https://doi.org/10.1016/j.icarus.2014.05.013>
- Dundas, C. M., & McEwen, A. S. (2015). Slope activity in Gale crater, Mars. *Icarus*, 254, 213–218. <https://doi.org/10.1016/j.icarus.2015.04.002>
- Dundas, C. M., McEwen, A. S., Chojnacki, M., Milazzo, M. P., Byrne, S., McElwaine, J. N., & Urso, A. (2017). Granular flows at recurring slope lineae on Mars indicate a limited role for liquid water. *Nature Geoscience*, 10, 903–907. <https://doi.org/10.1038/s41561-017-0012-510.1038/s41561-017-0012-5>
- Dundas, C. M., McEwen, A. S., Diniega, S., Byrne, S., & Martinez-Alonso, S. (2010). New and recent gully activity on Mars as seen by HiRISE. *Geophysical Research Letters*, 37, L07202. <https://doi.org/10.1029/2009GL041351>
- Dundas, C. M., McEwen, A. S., Diniega, S., Hansen, C. J., Byrne, S., & McElwaine, J. N. (2019). The formation of gullies on Mars today. *Geological Society, London, Special Publications*, 467, 67–94. <https://doi.org/10.1144/SP467.5>
- Dundas, C. M., Mellon, M. T., Conway, S. J., & Gastineau, R. (2019). Active boulder movement at high Martian latitudes. *Geophysical Research Letters*, 46, 5075–5082. <https://doi.org/10.1029/2019GL022993>
- Edgett, K. S., & Malin, M. C. (2000). New views of Mars eolian activity, materials, and surface properties: Three vignettes from the Mars Global Surveyor Mars Orbiter Camera. *Journal of Geophysical Research*, 105, 1623–1650. <https://doi.org/10.1029/1999JE001152>
- Edwards, C. S., & Piqueux, S. (2016). The water content of recurring slope lineae on Mars. *Geophysical Research Letters*, 43, 8912–8919. <https://doi.org/10.1002/2016GL070179>
- Ehlmann, B. R., & Edwards, C. S. (2014). Mineralogy of the Martian surface. *Annual Review of Earth and Planetary Sciences*, 42, 291–315. <https://doi.org/10.1146/annurev-earth-060313-055024>
- Fanara, L., Gwinner, K., Hauber, E., & Oberst, J. (2020). Present-day erosion rate of north polar scarps on Mars due to active mass wasting. *Icarus*, 342, 113434. <https://doi.org/10.1016/j.icarus.2019.113434>
- Fassett, C. I., & Head, J. W. (2008). Valley network-fed, open-basin lakes on Mars: Distribution and implications for Noachian surface and subsurface hydrology. *Icarus*, 198, 37–56. <https://doi.org/10.1016/j.icarus.2008.06.016>
- Fenton, L. K. (2006). Dune migration and slip face advancement in the Rabe crater dune field, Mars. *Geophysical Research Letters*, 33, L20201. <https://doi.org/10.1029/2006GL027133>
- Fenton, L. K., Michaels, T. I., & Chojnacki, M. (2015). Late Amazonian aeolian features, gradation, wind regimes, and sediment state in the vicinity of the Mars Exploration Rover Opportunity, Meridiani Planum, Mars. *Aeolian Research*, 16, 75–99. <https://doi.org/10.1016/j.aeolia.2014.11.004>
- Fischer, E. M., & Pieters, C. M. (1993). The continuum slope of Mars: Bidirectional reflectance investigations and applications to Olympus Mons. *Icarus*, 102, 185–202. <https://doi.org/10.1006/icar.1993.1043>
- Forget, F., Wordsworth, R., Millour, E., Madeleine, J.-B., Kerber, L., Leconte, J., et al. (2013). 3D modelling of the early Martian climate under a denser CO₂ atmosphere: Temperatures and CO₂ ice clouds. *Icarus*, 222, 81–99. <https://doi.org/10.1016/j.icarus.2012.10.019>
- Foroutan, M., Steinmetz, G., Zimbelman, J. R., & Duguay, C. R. (2019). Megaripples at Wau-an-Namus, Libya: A new analog for similar features on Mars. *Icarus*, 319, 840–851. <https://doi.org/10.1016/j.icarus.2018.10.021>
- Foroutan, M., & Zimbelman, J. R. (2016). Mega-ripples in Iran: A new analog for transverse aeolian ridges on Mars. *Icarus*, 274, 99–105. <https://doi.org/10.1016/j.icarus.2016.03.025>
- Gardin, E., Allemand, P., Quantin, C., & Thollot, P. (2010). Defrosting, dark flow features, and dune activity on Mars: Example in Russell crater. *Journal of Geophysical Research*, 115, E06016. <https://doi.org/10.1029/2009JE003515>
- Geissler, P. E. (2005). Three decades of Martian surface changes. *Journal of Geophysical Research*, 110, E02001. <https://doi.org/10.1029/2004JE002345>
- Geissler, P. E. (2014). The birth and death of transverse aeolian ridges on Mars. *Journal of Geophysical Research: Planets*, 119, 2583–2599. <https://doi.org/10.1002/2014je004633>
- Geissler, P. E., Fenton, L. K., Enga, M.-T., & Mukherjee, P. (2016). Orbital monitoring of Martian surface changes. *Icarus*, 278, 279–300. <https://doi.org/10.1016/j.icarus.2016.05.023>
- Geissler, P. E., Johnson, J. R., Sullivan, R., Herkenhoff, K., Mittlefehldt, D., Ferguson, R., et al. (2008). First in situ investigation of a dark wind streak on Mars. *Journal of Geophysical Research*, 113, E12S31. <https://doi.org/10.1029/2008JE003102>
- Geissler, P. E., Sullivan, R., Golombek, M., Johnson, J. R., Herkenhoff, K., Bridges, N., et al. (2010). Gone with the wind: Eolian erasure of the Mars Rover tracks. *Journal of Geophysical Research*, 115, E00F11. <https://doi.org/10.1029/2010JE003674>
- Giardini, D., Lognonné, P., Banerdt, W. B., Pike, W. T., Christensen, U., Ceylan, S., et al. (2020). The seismicity of Mars. *Nature Geoscience*, 13, 205–212. <https://doi.org/10.1038/s41561-020-0539-8>
- Golombek, M., Robinson, K., McEwen, A., Bridges, N., Ivanov, B., Tornabene, L., & Sullivan, R. (2010). Constraints on ripple migration at Meridiani Planum from Opportunity and HiRISE observations of fresh craters. *Journal of Geophysical Research*, 115, E00F08. <https://doi.org/10.1029/2010JE003628>
- Golombek, M. P., Grant, J. A., Crumpler, L. S., Greeley, R., Arvidson, R. E., Bell, J. F., III, et al. (2006). Erosion rates at the Mars Exploration Rover landing sites and long-term climate change on Mars. *Journal of Geophysical Research*, 111, E12S10. <https://doi.org/10.1029/2006JE002754>
- Grant, J. A., & Wilson, S. A. (2011). Late alluvial fan formation in southern Margaritifer Terra, Mars. *Geophysical Research Letters*, 38, L08201. <https://doi.org/10.1029/2011GL046844>
- Greeley, R., Arvidson, R., Bell, J. F., III, Christensen, P., Foley, D., Haldemann, A., et al. (2005). Martian variable features: New insights from the Mars Express orbiter and the Mars Exploration Rover Spirit. *Journal of Geophysical Research*, 110, E06002. <https://doi.org/10.1029/2005JE002403>
- Greeley, R., Waller, D. A., Cabrol, N. A., Landis, G. A., Lemmon, M. T., Neakrase, L. D. V., et al. (2010). Gusev crater, Mars: Observations of three dust devil seasons. *Journal of Geophysical Research*, 115, E00F02. <https://doi.org/10.1029/2010JE003608>
- Greeley, R., Whelley, P. L., Arvidson, R. E., Cabrol, N. A., Foley, D. J., Franklin, B. J., et al. (2006). Active dust devils in Gusev crater, Mars: Observations from the Mars Exploration Rover Spirit. *Journal of Geophysical Research*, 111, E12S09. <https://doi.org/10.1029/2006JE002743>
- Greeley, R., White, B., Leach, R., Iversen, J., & Pollack, J. (1976). Mars: Wind friction speeds for particle movement. *Geophysical Research Letters*, 3, 417–420. <https://doi.org/10.1029/GL003i008p00417>

- Grimm, R. E., Harrison, K. P., & Stillman, D. E. (2014). Water budgets of Martian recurring slope lineae. *Icarus*, 233, 316–327. <https://doi.org/10.1016/j.icarus.2013.11.013>
- Guinness, E. A., Leff, C. E., & Arvidson, R. E. (1982). Two Mars years of surface changes seen at the Viking landing sites. *Journal of Geophysical Research*, 87(10), 10051–10058. <https://doi.org/10.1029/JB087iB12p10051>
- Gulick, V. C., Glines, N., Hart, S., & Freeman, P. (2019). Geomorphological analysis of gullies on the central peak of Lyot Crater, Mars. *Geological Society, London, Special Publications*, 467, 233–265. <https://doi.org/10.1144/SP467.17>
- Hansen, C. J., Bourke, M., Bridges, N. T., Byrne, S., Colon, C., Diniega, S., et al. (2011). Seasonal erosion and restoration of Mars' northern polar dunes. *Science*, 331, 575–578. <https://doi.org/10.1126/science.1197636>
- Hansen, C. J., Bourke, M., McEwen, A., Mellon, M., Pommerol, A., Portyankina, G., & Thomas, N. (2012). Year 3 HiRISE observations of sublimation of the northern seasonal polar cap on Mars. Lunar and Planetary Science Conference 43, abstract #2386.
- Hansen, C. J., Byrne, S., Portyankina, G., Bourke, M., Dundas, C., McEwen, A., et al. (2013). Observations of the northern seasonal polar cap on Mars: I. Spring sublimation activity and processes. *Icarus*, 225, 881–897. <https://doi.org/10.1016/j.icarus.2012.09.024>
- Hansen, C. J., Diniega, S., Bridges, N., Byrne, S., Dundas, C., McEwen, A., & Portyankina, G. (2015). Agents of change on Mars' northern dunes: CO₂ ice and wind. *Icarus*, 251, 264–274. <https://doi.org/10.1016/j.icarus.2014.11.015>
- Hansen, C. J., Diniega, S., & Hayne, P. O. (2018). Mars' snowfall and sand avalanches. Lunar and Planetary Science Conference 49, abstract #2175.
- Hansen, C. J., Thomas, N., Portyankina, G., McEwen, A., Becker, T., Byrne, S., et al. (2010). HiRISE observations of gas sublimation-driven activity in Mars' southern polar regions: I. Erosion of the surface. *Icarus*, 205, 283–295. <https://doi.org/10.1016/j.icarus.2009.07.021>
- Harrison, T. N., Malin, M. C., & Edgett, K. S. (2009). *Liquid water on the surface of Mars today: Present gully activity observed by the Mars Reconnaissance Orbiter (MRO) and Mars Global Surveyor (MGS) and direction for future missions*. AGU Fall Meeting, abstract #P43D-1454.
- Hartmann, W. K., & Daubar, I. J. (2017). Martian cratering 11: Utilizing decimeter scale crater populations to study Martian history. *Meteoritics & Planetary Sciences*, 52, 493–510. <https://doi.org/10.1111/maps.12807>
- Hayne, P. O., Hansen, C. J., Byrne, S., Kass, D. M., Kleinböhl, A., Piqueux, S., et al. (2016). Snowfall variability and surface changes in the polar regions of Mars. Mars Polar Science Conference 6, abstract #6012.
- Heldmann, J. L., Conley, C. A., Brown, A. J., Fletcher, L., Bishop, J. L., & McKay, C. P. (2010). Possible liquid water origin for Atacama Desert mudflow and recent gully deposits on Mars. *Icarus*, 206, 685–690. <https://doi.org/10.1016/j.icarus.2009.09.013>
- Herkenhoff, K., Byrne, S., Dundas, C. M., Baugh, N. F., & Hunter, M. A. (2020). HiRISE observations of recent phenomena in the north polar region of Mars. 7th Mars Polar Science Conference, abstract #6059.
- Herkenhoff, K., Squyres, S. W., Arvidson, R., Bass, D. S., Bell, J. F., Bertelsen, P., et al. (2004). Textures of the soils and rocks at Gusev crater from Spirit's Microscopic Imager. *Science*, 305, 824–826. <https://doi.org/10.1126/science.110001510.1126/science.3050824>
- Heyer, T., Hiesinger, H., Reiss, D., Erkeling, G., Bernhardt, H., Luesebrink, D., & Jaumann, R. (2018). The Multi-Temporal Database of Planetary Image Data (MUTED): A web-based tool for studying dynamic Mars. *Planetary and Space Science*, 159, 56–65. <https://doi.org/10.1016/j.pss.2018.04.015>
- Heyer, T., Kreslavsky, M., Hiesinger, H., Reiss, D., Bernhardt, H., & Jaumann, R. (2019). Seasonal formation rates of Martian slope streaks. *Icarus*, 323, 76–86. <https://doi.org/10.1016/j.icarus.2019.01.010>
- Heyer, T., Raack, J., Hiesinger, H., & Jaumann, R. (2020). Dust devil triggering of slope streaks on Mars. *Icarus*, 351, 113951. <https://doi.org/10.1016/j.icarus.2020.113951>
- Horgan, B. H. N., & Bell, J. F. (2012). Seasonally active slipface avalanches in the north polar sand sea of Mars: Evidence for a wind-related origin. *Geophysical Research Letters*, 39, L09201. <https://doi.org/10.1029/2012GL051329>
- Horvath, D. G., Moitra, P., Hamilton, C. W., Craddock, R. A., & Andrews-Hanna, J. G. (2021). Evidence for geologically recent explosive volcanism in Elysium Planitia, Mars. *Icarus*, 364, 114499. <https://doi.org/10.1016/j.icarus.2021.114499>
- Ivanov, B. A. (2001). Mars/Moon cratering rate ratio estimates. In *Chronology and evolution of Mars* (pp. 87–104). Kluwer Academic Publishers. https://doi.org/10.1007/978-94-017-1035-0_4
- Jakosky, B. M., Slipski, M., Benna, M., Mahaffy, P., Elrod, M., Yelle, R., et al. (2017). Mars' atmospheric history derived from upper-atmosphere measurements of ³⁸Ar/³⁶Ar. *Science*, 355, 1408–1410. <https://doi.org/10.1126/science.aai7721>
- JeongAhn, Y., & Malhotra, R. (2015). The current impact flux on Mars and its seasonal variation. *Icarus*, 262, 140–153. <https://doi.org/10.1016/j.icarus.2015.08.032>
- Jones, K. L., Arvidson, R. E., Guinness, E. A., Bragg, S. L., Wall, S. D., Carlston, C. E., & Pidek, D. G. (1979). One Mars year: Viking Lander imaging observations. *Science*, 204, 799–806. <https://doi.org/10.1126/science.204.4395.799>
- Jouannic, G., Conway, S. J., Gargani, J., Costard, F., Massé, M., Bourgeois, O., et al. (2019). Morphological characterization of landforms produced by springtime seasonal activity on Russell crater megadune, Mars. *Geological Society, London, Special Publications*, 467, 115–144. <https://doi.org/10.1144/SP467.16>
- Kereszturi, A., Möhlmann, D., Berczi, S., Ganti, T., Horvath, A., Kuti, A., et al. (2010). Indications of brine related local seepage phenomena on the northern hemisphere of Mars. *Icarus*, 207, 149–164. <https://doi.org/10.1016/j.icarus.2009.10.012>
- Kereszturi, A., Möhlmann, D., Berczi, S., Ganti, T., Kuti, A., Sik, A., & Horvath, A. (2009). Recent rheological processes on dark polar dunes of Mars: Driven by interfacial water? *Icarus*, 201, 492–503. <https://doi.org/10.1016/j.icarus.2009.01.014>
- Kereszturi, A., Möhlmann, D., Berczi, S., Horvath, A., Sik, A., & Szathmary, E. (2011). Possible role of brines in the darkening and flow-like features on the Martian polar dunes based on HiRISE images. *Planetary and Space Science*, 59, 1413–1427. <https://doi.org/10.1016/j.pss.2011.05.012>
- Khuller, A. R., & Christensen, P. R. (2021). Evidence of exposed dusty water ice within Martian gullies. *Journal of Geophysical Research: Planets*, 126, e2020JE006539. <https://doi.org/10.1029/2020JE006539>
- Kieffer, H. H. (1990). H₂O grain size and the amount of dust in Mars' residual north polar cap. *Journal of Geophysical Research*, 95, 1481–1493. <https://doi.org/10.1029/JB095iB02p01481>
- Kieffer, H. H. (2007). Cold jets in the Martian polar caps. *Journal of Geophysical Research*, 112, E08005. <https://doi.org/10.1029/2006JE002816>
- Kieffer, H. H. (2013). Thermal model for analysis of Mars infrared mapping. *Journal of Geophysical Research: Planets*, 118, 451–470. <https://doi.org/10.1029/2012JE004164>
- Kieffer, H. H., Christensen, P. R., & Titus, T. N. (2006). CO₂ jets formed by sublimation beneath translucent slab ice in Mars' seasonal south polar cap. *Nature*, 442, 793–796. <https://doi.org/10.1038/nature04945>
- Kinch, K. M., Bell, J. F., Goetz, W., Johnson, J. R., Joseph, J., Madsen, M. B., & Solh-Dickstein, J. (2015). Dust deposition on the decks of the Mars Exploration Rovers: 10 years of dust dynamics on the Panoramic Camera calibration targets. *Earth and Space Science*, 2, 144–172. <https://doi.org/10.1002/2014EA000073>

- Kite, E. S., Williams, J.-P., Lucas, A., & Aharonson, O. (2014). Low palaeopressure of the Martian atmosphere estimated from the size distribution of ancient craters. *Nature Geoscience*, 7, 335–339. <https://doi.org/10.1038/NNGEO2137>
- Knutsen, E. W., Villanueva, G. L., Liuzzi, G., Crismani, M. M. J., Mumma, M. J., Smith, M. D., et al. (2021). Comprehensive investigation of Mars methane and organics with ExoMars/NOMAD. *Icarus*, 357, 114266. <https://doi.org/10.1016/j.icarus.2020.114266>
- Kok, J. F. (2010). Difference in the wind speeds required for initiation versus continuation of sand transport on mars: Implications for dunes and dust storms. *Physical Review Letters*, 104, 074502. <https://doi.org/10.1103/PhysRevLett.104.074502>
- Korablev, O., Vandaele, A. C., Montmessin, F., Fedorova, A. A., Trokhimovskiy, A., Forget, F., et al. (2019). No detection of methane on Mars from early ExoMars Trace Gas Orbiter observations. *Nature*, 568, 517–520. <https://doi.org/10.1038/s41586-019-1096-4>
- Kumar, P. S., Krishna, N., Prasanna Lakshmi, K. J., Raghukanth, S. T. G., Dhabu, A., & Platz, T. (2019). Recent seismicity in Valles Marineris, Mars: Insights from young faults, landslides, boulder falls and possible mud volcanoes. *Earth and Planetary Science Letters*, 505, 51–64. <https://doi.org/10.1016/j.epsl.2018.10.008>
- Landis, M. E., Byrne, S., Daubar, I. J., Herkenhoff, K. E., & Dundas, C. M. (2016). A revised surface age for the north polar layered deposits of Mars. *Geophysical Research Letters*, 43, 3060–3068. <https://doi.org/10.1002/2016GL068434>
- Landis, M. E., Byrne, S., Hayne, P. O., & Piqueux, S. (2021). *Interannual variability of ice within north polar layered deposits craters on Mars*. Lunar and Planetary Science Conference 52, abstract #1653.
- Langevin, Y., Poulet, F., Bibring, J.-P., Schmitt, B., Douté, S., & Gondet, B. (2005). Summer evolution of the north polar cap of Mars as observed by OMEGA/Mars Express. *Science*, 307, 1581–1584. <https://doi.org/10.1126/science.1109438>
- Lapotre, M., Ewing, R. C., Lamb, M. P., Fischer, W. W., Grotzinger, J. P., Rubin, D. M., et al. (2016). Large wind ripples on Mars: A record of atmospheric evolution. *Science*, 353, 55–58. <https://doi.org/10.1126/science.aaf3206>
- Lapotre, M. G. A., Ewing, R. C., Weitz, C. M., Lewis, K. W., Lamb, M. P., Ehlmann, B. L., & Rubin, D. C. (2018). Morphologic diversity of Martian ripples: Implications for large-ripple formation. *Geophysical Research Letters*, 45, 10229–10239. <https://doi.org/10.1029/2018GL079029>
- Laskar, J., Correia, A. C. M., Gastineau, M., Joutel, F., Levrard, B., & Robutel, P. (2004). Long term evolution and chaotic diffusion of the insolation quantities of Mars. *Icarus*, 170, 343–364. <https://doi.org/10.1016/j.icarus.2004.04.005>
- Leask, E. K., Ehlmann, B. L., Dundar, M. M., Murchie, S. L., & Seelos, F. P. (2018). Challenges in the search for perchlorate and other hydrated minerals with 2.1-mm absorptions on Mars. *Geophysical Research Letters*, 45, 12180–12189. <https://doi.org/10.1029/2018GL080077>
- Leighton, R. B., & Murray, B. C. (1966). Behavior of carbon dioxide and other volatiles on Mars. *Science*, 153, 136–144. <https://doi.org/10.1126/science.153.3732.136>
- Lemmon, M. T., Newman, C. E., Renno, N., Mason, E., Battalio, M., Richardson, M. I., & Kahanpää, H. (2017). *Dust devil activity at the Curiosity Mars rover field site*. Lunar and Planetary Science Conference 48, abstract #2952.
- Levy, J. (2012). Hydrological characteristics of recurrent slope lineae on Mars: Evidence for liquid flow through regolith and comparisons with Antarctic terrestrial analogs. *Icarus*, 219, 1–4. <https://doi.org/10.1016/j.icarus.2012.02.016>
- Lorenz, R. D., & Reiss, D. (2015). Solar panel clearing events, dust devil tracks, and in-situ vortex detections on Mars. *Icarus*, 248, 162–164. <https://doi.org/10.1016/j.icarus.2014.10.034>
- Mahaffy, P. R., Webster, C. R., Stern, J. C., Brunner, A. E., Atreya, S. K., Conrad, P. G., et al. (2015). The imprint of atmospheric evolution in the D/H of Hesperian clay minerals on Mars. *Science*, 347, 412–414. <https://doi.org/10.1126/science.1260291>
- Malin, M. C., Bell, J. F., Cantor, B. A., Caplinger, M. A., Calvin, W. M., Clancy, R. T., et al. (2007). Context Camera investigation on board the Mars Reconnaissance Orbiter. *Journal of Geophysical Research*, 112, E05S04. <https://doi.org/10.1029/2006JE002808>
- Malin, M. C., Caplinger, M. A., & Davis, S. D. (2001). Observational evidence for an active surface reservoir of solid carbon dioxide on Mars. *Science*, 294, 2146–2148. <https://doi.org/10.1126/science.1066416>
- Malin, M. C., Danielson, G. E., Ingersoll, A. P., Masursky, H., Veverka, J., Ravine, M. A., & Soulanille, T. A. (1992). Mars Observer Camera. *Journal of Geophysical Research*, 97, 7699–7718. <https://doi.org/10.1029/92JE00340>
- Malin, M. C., & Edgett, K. S. (2000). Evidence for recent groundwater seepage and surface runoff on Mars. *Science*, 288, 2330–2335. <https://doi.org/10.1126/science.288.5475.2330>
- Malin, M. C., & Edgett, K. S. (2001). Mars Global Surveyor Mars Orbiter Camera: Interplanetary cruise through primary mission. *Journal of Geophysical Research*, 106, 23429–23570. <https://doi.org/10.1029/2000JE001455>
- Malin, M. C., Edgett, K. S., Cantor, B. A., Caplinger, M. A., Danielson, G. E., Jensen, E. H., et al. (2010). An overview of the 1985-2006 Mars Orbiter Camera science investigation. *Mars, The International Journal of Mars Science and Exploration*, 5, 1–60. <https://doi.org/10.1555/mars.2010.0001>
- Malin, M. C., Edgett, K. S., Posiolova, L. V., McColley, S. M., & Noe Dobrea, E. Z. (2006). Present-day cratering rate and contemporary gully activity on Mars. *Science*, 314, 1573–1577. <https://doi.org/10.1126/science.1135156>
- Mangold, N., Costard, F., & Forget, F. (2003). Debris flows over sand dunes on Mars: Evidence for liquid water. *Journal of Geophysical Research*, 108, 5027. <https://doi.org/10.1029/2002JE001958>
- Martin, L. J., James, P. B., Dollfus, A., Iwasaki, K., & Beish, J. D. (1992). Telescopic observations: Visual, photographic, polarimetric. In *Mars* (pp. 34–70). University of Arizona Press.
- Martínez, G. M., Fischer, E., Rennó, N. O., Sebastián, E., Kempainen, O., Bridges, N., et al. (2016). Likely frost events at Gale crater: Analysis from MSL/REMS measurements. *Icarus*, 280, 93–102. <https://doi.org/10.1016/j.icarus.2015.12.004>
- Martínez, G. M., Newman, C. N., De Vicente-Retortillo, A., Fischer, E., Renno, N. O., Richardson, M. I., et al. (2017). The modern near-surface Martian climate: A review of in-situ meteorological data from Viking to Curiosity. *Space Science Reviews*, 212, 295–338. <https://doi.org/10.1007/s11214-017-0360-x>
- McClung, D., & Schaerer, P. A. (2006). *The avalanche handbook* (3rd ed.).
- McEwen, A. S., Dundas, C. M., Mattson, S. S., Toigo, A. D., Ojha, L., Wray, J. J., et al. (2014). Recurring slope lineae in equatorial regions of Mars. *Nature Geoscience*, 7, 53–58. <https://doi.org/10.1038/ngeo2014>
- McEwen, A. S., Eliason, E. M., Bergstrom, J. W., Bridges, N. T., Hansen, C. J., Delamere, W. A., et al. (2007). Mars Reconnaissance Orbiter's High Resolution Imaging Science Experiment. *Journal of Geophysical Research*, 112, E05S02. <https://doi.org/10.1029/2005JE002605>
- McEwen, A. S., Ojha, L., Dundas, C. M., Mattson, S. S., Byrne, S., Wray, J. J., et al. (2011). Seasonal flows on warm Martian slopes. *Science*, 333, 740–743. <https://doi.org/10.1126/science.1204816>
- McEwen, A. S., Schaefer, E. I., Sutton, S. S., Tamppari, L. K., Chojnacki, M., & Chojnacki, M. (2021). Mars: Abundant recurring slope lineae (RSL) following the Planet-Encircling Dust Event (PEDE) of 2018. *Journal of Geophysical Research: Planets*, 126. <https://doi.org/10.1029/2020JE006575>
- McKeown, L. E., Bourke, M. C., & McElwaine, J. N. (2017). Experiments on sublimating carbon dioxide ice and implications for contemporary surface processes on Mars. *Scientific Reports*, 7, 14181. <https://doi.org/10.1038/s41598-017-14132-2>

- Mellon, M. T., Arvidson, R. E., Marlow, J. J., Phillips, R. J., & Asphaug, E. (2008). Periglacial landforms at the Phoenix landing site and the northern plains of Mars. *Journal of Geophysical Research*, *113*, E00A23. <https://doi.org/10.1029/2007JE003039>
- Mellon, M. T., Malin, M. C., Arvidson, R. E., Searls, M. L., Sizemore, H. G., Heet, T. L., et al. (2009). The periglacial landscape at the Phoenix landing site. *Journal of Geophysical Research*, *114*, E00E06. <https://doi.org/10.1029/2009JE003418>
- MGS MOC Release MOC2-1220. (2005). *8 Years at Mars #1: New dune gullies*. Retrieved from http://www.msss.com/mars_images/moc/2005/09/20/dunegullies/
- MGS MOC Release MOC2-1222. (2005). *8 Years at Mars #3: Rolling stones make new boulder tracks*. Retrieved from https://www.msss.com/mars_images/moc/2005/09/20/bouldertracks/index.html
- Moore, H. J. (1985). The Martian dust storm of Sol 1742. *Journal of Geophysical Research*, *90*, D163–D174. <https://doi.org/10.1029/JB090iS01p00163>
- Moore, H. J., Hutton, R. E., Clow, G. D., & Spitzer, C. R. (1987). *Physical properties of the surface materials at the Viking landing sites on Mars*. U.S. Geological Survey Professional Paper 1389. <https://doi.org/10.3133/pp1389>
- Morris, E. C. (1982). Aureole deposits of the Martian volcano Olympus Mons. *Journal of Geophysical Research*, *87*, 1164–1178. <https://doi.org/10.1029/JB087iB02p01164>
- Mumma, M. J., Villanueva, G. L., Novak, R. E., Hewagama, T., Boney, B. P., DiSanti, M. A., et al. (2009). Strong release of methane on Mars in northern summer 2003. *Science*, *323*, 1041–1045. <https://doi.org/10.1126/science.1165243>
- Munaretto, G., Pajola, M., Cremonese, G., Re, C., Lucchetti, A., Simioni, E., et al. (2020). Implications for the origin and evolution of Martian recurring slope lineae at Hale crater from CaSSIS observations. *Planetary and Space Science*, *187*, 104947. <https://doi.org/10.1016/j.pss.2020.104947>
- Murchie, S., Arvidson, R., Bedini, P., Beisser, K., Bibring, J.-P., Bishop, J., et al. (2007). Compact Reconnaissance Imaging Spectrometer for Mars (CRISM) on Mars Reconnaissance Orbiter (MRO). *Journal of Geophysical Research*, *112*, E05S03. <https://doi.org/10.1029/2006JE002682>
- Mushkin, A., Gillespie, A. R., Montgomery, D. R., Schreiber, C., & Arvidson, R. E. (2010). Spectral constraints on the composition of low-albedo slope streaks in the Olympus Mons Aureole. *Geophysical Research Letters*, *37*, L22201. <https://doi.org/10.1029/2010GL044535>
- Mutch, T. A., Arvidson, R. E., Binder, A. B., Guinness, E. A., & Morris, E. C. (1977). The geology of the Viking Lander 2 site. *Journal of Geophysical Research*, *82*, 4452–4467. <https://doi.org/10.1029/JG082i028p04452>
- Neakrase, L. D. V., Balme, M. R., Esposito, F., Kelling, T., Klose, M., Kok, J. F., et al. (2016). Particle lifting processes in dust devils. *Space Science Reviews*, *203*, 347–376. <https://doi.org/10.1007/s11214-016-0296-6>
- Ojha, L., Chojnacki, M., McDonald, G. D., Shumway, A., Wolff, M. J., Smith, M. D., et al. (2017). Seasonal slumps in Juventae Chasma, Mars. *Journal of Geophysical Research: Planets*, *122*, 2193–2214. <https://doi.org/10.1002/2017JE005375>
- Ojha, L., McEwen, A., Dundas, C., Byrne, S., Mattson, S., Wray, J., et al. (2014). HiRISE observations of recurring slope lineae (RSL) during southern summer on Mars. *Icarus*, *231*, 365–376. <https://doi.org/10.1016/j.icarus.2013.12.021>
- Ojha, L., Wilhelm, M. B., Murchie, S. L., McEwen, A. S., Wray, J. J., Hanley, J., et al. (2015). Spectral evidence for hydrated salts in recurring slope lineae on Mars. *Nature Geoscience*, *8*, 829–832. <https://doi.org/10.1038/NNGEO2546>
- Ojha, L., Wray, J. J., Murchie, S. L., McEwen, A. S., Wolff, M. J., & Karunatillake, S. (2013). Spectral constraints on the formation mechanism of recurring slope lineae. *Geophysical Research Letters*, *40*, 5621–5626. <https://doi.org/10.1002/2013GL057893>
- Orosei, R., Lauro, S. E., Pettinelli, E., Cicchetti, A., Coradini, M., Cosciotti, B., et al. (2018). Radar evidence of subglacial liquid water on Mars. *Science*, *361*, 490–493. <https://doi.org/10.1126/science.aar7268>
- Pasquon, K., Gargani, J., Massé, M., & Conway, S. J. (2016). Present-day formation and seasonal evolution of linear dune gullies on Mars. *Icarus*, *274*, 195–210. <https://doi.org/10.1016/j.icarus.2016.03.024>
- Pasquon, K., Gargani, J., Massé, M., Vincendon, M., Conway, S. J., Séjourné, A., et al. (2019). Present-day development of gully-channel sinuosity by carbon dioxide gas supported flows on Mars. *Icarus*, *329*, 296–313. <https://doi.org/10.1016/j.icarus.2019.03.034>
- Pasquon, K., Gargani, J., Nachon, M., Conway, S. J., Massé, M., Jouannic, G., et al. (2019). Are different Martian gully morphologies due to different processes on the Kaiser dune field? *Geological Society, London, Special Publications*, *467*, 145–164. <https://doi.org/10.1144/SP467.13>
- Pelletier, J. D., Kolb, K. J., McEwen, A. S., & Kirk, R. L. (2008). Recent bright gully deposits on Mars: Wet or dry flow? *Geology*, *36*, 211–214. <https://doi.org/10.1130/G24346A.1>
- Perrin, C., Rodriguez, S., Jacob, A., Lucas, A., Spiga, A., Murdoch, N., et al. (2020). Monitoring of dust devil tracks around the InSight landing site, Mars, and comparison with in situ atmospheric data. *Geophysical Research Letters*, *47*, e2020GL087234. <https://doi.org/10.1029/2020GL087234>
- Piqueux, S., Byrne, S., Kieffer, H. H., Titus, T. N., & Hansen, C. J. (2015). Enumeration of Mars years and seasons since the beginning of telescopic exploration. *Icarus*, *251*, 332–338. <https://doi.org/10.1016/j.icarus.2014.12.014>
- Piqueux, S., Byrne, S., & Richardson, M. I. (2003). Sublimation of Mars's southern seasonal CO₂ ice cap and the formation of spiders. *Journal of Geophysical Research*, *108*. <https://doi.org/10.1029/2002JE002007>
- Piqueux, S., & Christensen, P. R. (2008). North and south subice gas flow and venting of the seasonal caps of Mars: A major geomorphological agent. *Journal of Geophysical Research*, *113*, E06005. <https://doi.org/10.1029/2007JE003009>
- Piqueux, S., Kleinböhl, A., Hayne, P. O., Heavens, N. G., Kass, D. M., McCleese, D. J., et al. (2016). Discovery of a widespread low-latitude diurnal CO₂ frost cycle on Mars. *Journal of Geophysical Research: Planets*, *121*, 1174–1189. <https://doi.org/10.1002/2016JE005034>
- Piqueux, S., Kleinböhl, A., Hayne, P. O., Kass, D. M., Schofield, J. T., & McCleese, D. J. (2015). Variability of the Martian seasonal CO₂ cap extent over eight Mars Years. *Icarus*, *251*, 164–180. <https://doi.org/10.1016/j.icarus.2014.10.045>
- Portyankina, G., Hansen, C. J., & Aye, K.-M. (2017). Present-day erosion of Martian polar terrain by the seasonal CO₂ jets. *Icarus*, *282*, 93–103. <https://doi.org/10.1016/j.icarus.2016.09.007>
- Portyankina, G., Markiewicz, W. J., Thomas, N., Hansen, C. J., & Milazzo, M. (2010). HiRISE observations of gas sublimation-driven activity in Mars' southern polar regions: III. Models of processes involving translucent ice. *Icarus*, *205*, 311–320. <https://doi.org/10.1016/j.icarus.2009.08.029>
- Portyankina, G., Pommerol, A., Aye, K.-M., Hansen, C. J., & Thomas, N. (2012). Polygonal cracks in the seasonal semi-translucent CO₂ ice layer in Martian polar areas. *Journal of Geophysical Research*, *117*, E02006. <https://doi.org/10.1029/2011JE003917>
- Raack, J., Conway, S. J., Heyer, T., Bickel, V. T., Philippe, M., Hiesinger, H., et al. (2020). Present-day gully activity in Sisyphi Cavi, Mars—Flow-like features and block movements. *Icarus*, *350*, 113899. <https://doi.org/10.1016/j.icarus.2020.113899>
- Raack, J., Reiss, D., Appéré, T., Vincendon, M., Ruesch, O., & Hiesinger, H. (2015). Present-day seasonal gully activity in a south polar pit (Sisyphi Cavi) on Mars. *Icarus*, *251*, 226–243. <https://doi.org/10.1016/j.icarus.2014.03.040>

- Reiss, D., Erkeling, G., Bauch, K. E., & Hiesinger, H. (2010). Evidence for present day gully activity on the Russell crater dune field, Mars. *Geophysical Research Letters*, *37*, L06203. <https://doi.org/10.1029/2009GL042192>
- Reiss, D., Fenton, L., Neakrase, L., Zimmerman, M., Statella, T., Whelley, P., et al. (2016). Dust devil tracks. *Space Science Reviews*, *203*, 143–181. <https://doi.org/10.1007/s11214-016-0308-6>
- Reiss, D., & Jaumann, R. (2003). Recent debris flows on Mars: Seasonal observations of the Russell crater dune field. *Geophysical Research Letters*, *30*, 1321. <https://doi.org/10.1029/2002GL016704>
- Reiss, D., Lorenz, R. D., Balme, M., Neakrase, L. D., Rossi, A. P., Spiga, A., & Zarnecki, J. (2016). Editorial: Topical volume on dust devils. *Space Science Reviews*, *203*, 1–4. <https://doi.org/10.1007/s11214-016-0314-8>
- Reiss, D., Raack, J., & Hiesinger, H. (2011). Bright dust devil tracks on Earth: Implications for their formation on Mars. *Icarus*, *211*, 917–920. <https://doi.org/10.1016/j.icarus.2010.09.009>
- Reiss, D., Spiga, A., & Erkeling, G. (2014). The horizontal motion of dust devils on Mars derived from CRISM and CTX/HIRISE observations. *Icarus*, *227*, 8–20. <https://doi.org/10.1016/j.icarus.2013.08.028>
- Roback, K. P., Runyon, K. D., Avouac, J. P., Newman, C. E., & Ayoub, F. (2019). *Understanding ripple and whole-dune motion at active Martian dune fields*. Lunar and Planetary Science Conference 50, abstract #3169.
- Roberts, G. P., Crawford, I. A., Peacock, D., Vetterlein, J., Parfitt, E., & Bishop, L. (2007). Possible evidence for on-going volcanism on Mars as suggested by thin, elliptical sheets of low-albedo particulate material around pits and fissures close to Cerberus Fossae. *Earth, Moon, and Planets*, *101*, 1–16. <https://doi.org/10.1007/s11038-007-9140-z>
- Roberts, G. P., Matthews, B., Bristow, C., Guerrieri, L., & Vetterlein, J. (2012). Possible evidence of paleomarsquakes from fallen boulder populations, Cerberus Fossae, Mars. *Journal of Geophysical Research*, *117*, E02009. <https://doi.org/10.1029/2011JE003816>
- Rodriguez, J. A. P., Tanaka, K. L., Langevin, Y., Bourke, M., Kargel, J., Christensen, P., & Sasaki, S. (2007). Recent aeolian erosion and deposition in the north polar plateau of Mars. *Mars, The International Journal of Mars Science and Exploration*, *3*, 29–41. <https://doi.org/10.1555/mars.2007.0003>
- Rummel, J. D., Beaty, D. W., Jones, M. A., Bakermans, C., Barlow, N. G., Boston, P. J., et al. (2014). A new analysis of Mars “special regions”: Findings of the second MEPAG special regions science analysis group (SR-SAG2). *Astrobiology*, *14*(11), 887–968. <https://doi.org/10.1089/ast.2014.1227>
- Runyon, K. D., Bridges, N. T., Ayoub, F., Newman, C. E., & Quade, J. J. (2017). An integrated model for dune morphology and sand fluxes on Mars. *Earth and Planetary Science Letters*, *457*, 204–212. <https://doi.org/10.1016/j.epsl.2016.09.054>
- Russell, P. S., Feleke, S., & Byrne, S. (2014). *Landslide erosion rates of north polar layered deposit cliffs and the underlying basal unit*. Eighth International Conference on Mars, abstract #1373.
- Russell, P. S., Thomas, N., Byrne, S., Herkenhoff, K., Fishbaugh, K., Bridges, N., et al. (2008). Seasonally active frost-dust avalanches on a north polar scarp of Mars captured by HiRISE. *Geophysical Research Letters*, *35*, L23204. <https://doi.org/10.1029/2008GL035790>
- Sagan, C., Veveřka, J., Fox, P., Dubisch, R., French, R., Gierasch, P., et al. (1973). Variable features on Mars, 2, Mariner 9 global results. *Journal of Geophysical Research*, *78*, 4163–4196. <https://doi.org/10.1029/JB078i020p04163>
- Sagan, C., Veveřka, J., Fox, P., Dubisch, R., Lederburg, J., Levinthal, E., et al. (1972). Variable features on Mars: Preliminary Mariner 9 television results. *Icarus*, *17*, 346–372. [https://doi.org/10.1016/0019-1035\(72\)90005-X](https://doi.org/10.1016/0019-1035(72)90005-X)
- Schaefer, E. I., McEwen, A. S., & Sutton, S. S. (2019). A case study of recurring slope lineae (RSL) at Tivat crater: Implications for RSL origins. *Icarus*, *317*, 621–648. <https://doi.org/10.1016/j.icarus.2018.07.014>
- Scheller, E. L., Ehlmann, B. L., Hu, R., Adams, D. J., & Yung, Y. L. (2021). Long-term drying of Mars by sequestration of ocean-scale volumes of water in the crust. *Science*, *372*, 56–62. <https://doi.org/10.1126/science.abc7717>
- Schorghofer, N., Aharonson, O., Gerstell, M. F., & Tatsumi, L. (2007). Three decades of slope streak activity on Mars. *Icarus*, *191*, 132–140. <https://doi.org/10.1016/j.icarus.2007.04.026>
- Schorghofer, N., & King, C. M. (2011). Sporadic formation of slope streaks on Mars. *Icarus*, *216*, 159–168. <https://doi.org/10.1016/j.icarus.2011.08.028>
- Silvestro, S., Chojnacki, M., Vaz, D. A., Cardinale, M., Yizhaq, H., & Esposito, F. (2020). Megaripple migration on Mars. *Journal of Geophysical Research: Planets*, *125*, e2020JE006446. <https://doi.org/10.1029/2020JE006446>
- Silvestro, S., Fenton, L. K., Vaz, D. A., Bridges, N. T., & Ori, G. G. (2010). Ripple migration and dune activity on Mars: Evidence for dynamic wind processes. *Geophysical Research Letters*, *37*, L20203–n. <https://doi.org/10.1029/2010GL044743>
- Silvestro, S., Vaz, D. A., Di Achille, G., Popa, I. C., & Esposito, F. (2015). Evidence for different episodes of aeolian construction and a new type of wind streak in the 2016 ExoMars landing ellipse in Meridiani Planum, Mars: Aeolian processes in Meridiani Planum. *Journal of Geophysical Research: Planets*, *120*, 760–774. <https://doi.org/10.1002/2014JE004756>
- Smith, I. B., Diniega, S., Beaty, D. W., Thorsteinsson, T., Becerra, P., Bramson, A. M., et al. (2018). 6th International Conference on Mars Polar Science and Exploration: Conference summary and five top questions. *Icarus*, *308*, 2–14. <https://doi.org/10.1016/j.icarus.2017.06.027>
- Smith, I. B., Hayne, P. O., Byrne, S., Becerra, P., Kahre, M., Calvin, W., et al. (2020). The Holy Grail: A road map for unlocking the climate record stored within Mars’ polar layered deposits. *Planetary and Space Science*, *184*, 104841. <https://doi.org/10.1016/j.pss.2020.104841>
- Smith, M. D. (2008). Spacecraft observations of the Martian atmosphere. *Annual Review of Earth and Planetary Sciences*, *36*, 191–219. <https://doi.org/10.1146/annurev.earth.36.031207.124334>
- Sori, M. M., & Bramson, A. M. (2019). Water on Mars, with a grain of salt: Local heat anomalies are required for basal melting of ice at the south pole today. *Geophysical Research Letters*, *46*, 1222–1231. <https://doi.org/10.1029/2018GL080985>
- Sori, M. M., Byrne, S., & Bramson, A. M. (2017). *Present-day flow rates of mid-latitude glaciers on Mars*. European Planetary Science Congress, abstract #382.
- Sori, M. M., Byrne, S., Hamilton, C. W., & Landis, M. E. (2016). Viscous flow rates of icy topography on the north polar layered deposits of Mars. *Geophysical Research Letters*, *43*, 541–549. <https://doi.org/10.1002/2015GL067298>
- Speyerer, E. J., Povilaitis, R. Z., Robinson, M. S., Thomas, P. C., & Wagner, R. V. (2016). Quantifying crater production and regolith overturn on the Moon with temporal imaging. *Nature*, *538*, 215–218. <https://doi.org/10.1038/nature19829>
- Stanzel, C., Pätzold, M., Williams, D. A., Whelley, P. L., Greeley, R., & Neukum, G., & HRSC Co-Investigator Team. (2008). Dust devil speeds, directions of motion and general characteristics observed by the Mars Express High Resolution Stereo Camera. *Icarus*, *197*, 39–51. <https://doi.org/10.1016/j.icarus.2008.04.017>
- Stillman, D. E. (2018). Unraveling the mysteries of recurring slope lineae. In *Dynamic Mars* (pp. 51–85). Elsevier Books. <https://doi.org/10.1016/B978-0-12-813018-6.00002-9>
- Stillman, D. E., Bue, B. D., Wagstaff, K. L., Primm, K. M., Michaels, T. I., & Grimm, R. E. (2020). Evaluation of wet and dry recurring slope lineae (RSL) formation mechanisms based on quantitative mapping of RSL in Gari Crater, Valles Marineris, Mars. *Icarus*, *335*, 113420. <https://doi.org/10.1016/j.icarus.2019.113420>

- Stillman, D. E., & Grimm, R. E. (2018). Two pulses of seasonal activity in Martian southern mid-latitude recurring slope lineae (RSL). *Icarus*, 302, 126–133. <https://doi.org/10.1016/j.icarus.2017.10.026>
- Stillman, D. E., Michaels, T. I., & Grimm, R. E. (2017). Characteristics of the numerous and widespread recurring slope lineae (RSL) in Valles Marineris, Mars. *Icarus*, 285, 195–210. <https://doi.org/10.1016/j.icarus.2016.10.025>
- Stillman, D. E., Michaels, T. I., Grimm, R. E., & Hanley, J. (2016). Observations and modeling of northern mid-latitude recurring slope lineae (RSL) suggest recharge by a present-day Martian briny aquifer. *Icarus*, 265, 125–138. <https://doi.org/10.1016/j.icarus.2015.10.007>
- Stillman, D. E., Michaels, T. I., Grimm, R. E., & Harrison, K. P. (2014). New observations of Martian southern mid-latitude recurring slope lineae (RSL) imply formation by freshwater subsurface flows. *Icarus*, 233, 328–341. <https://doi.org/10.1016/j.icarus.2014.01.017>
- Sullivan, R., Arvidson, R., Bell, J. F., Gellert, R., Golombek, M., Greeley, R., et al. (2008). Wind-driven particle mobility on Mars: Insights from Mars Exploration Rover observations at “El Dorado” and surroundings at Gusev crater. *Journal of Geophysical Research*, 113, E06S07. <https://doi.org/10.1029/2008je003101>
- Sullivan, R., Banfield, D., Bell, J. F., Calvin, W., Fike, D., Golombek, M., et al. (2005). Aeolian processes at the Mars Exploration Rover Meridiani Planum landing site. *Nature*, 436, 58–61. <https://doi.org/10.1038/nature03641>
- Sullivan, R., & Kok, J. (2017). Aeolian saltation on Mars at low wind speeds. *Journal of Geophysical Research: Planets*, 122, 2111–2143. <https://doi.org/10.1002/2017JE005275>
- Sullivan, R., Kok, J. F., Katra, I., & Yizhaq, H. (2020). A broad continuum of aeolian impact ripple morphologies on Mars is enabled by low wind dynamic pressures. *Journal of Geophysical Research: Planets*, 125. <https://doi.org/10.1029/2020JE006485>
- Sullivan, R., Thomas, P., Veverka, J., Malin, M., & Edgett, K. S. (2001). Mass movement slope streaks imaged by the Mars Orbiter Camera. *Journal of Geophysical Research*, 106, 23607–23633. <https://doi.org/10.1029/2000JE001296>
- Szwast, M. A., Richardson, M. I., & Vasavada, A. R. (2006). Surface dust redistribution on Mars as observed by the Mars Global Surveyor and Viking orbiters. *Journal of Geophysical Research*, 111, E11008. <https://doi.org/10.1029/2005JE002485>
- Tebolt, M., Levy, J., Goudge, T., & Schorghofer, N. (2020). Slope, elevation, and thermal inertia trends of Martian recurring slope lineae initiation and termination points: Multiple possible processes occurring on coarse, sandy slopes. *Icarus*, 338, 113536. <https://doi.org/10.1016/j.icarus.2019.113536>
- Tesson, P.-A., Conway, S. J., Mangold, N., Ciazela, J., Lewis, S. R., & Mége, D. (2020). Evidence for thermal-stress-induced rockfalls on Mars impact crater slopes. *Icarus*, 342, 113503. <https://doi.org/10.1016/j.icarus.2019.113503>
- Thomas, M. F., McEwen, A. S., & Dundas, C. M. (2020). Present-day mass wasting in sulfate-rich sediments in the equatorial regions of Mars. *Icarus*, 342, 113566. <https://doi.org/10.1016/j.icarus.2019.113566>
- Thomas, N., Cremonese, G., Ziethe, R., Gerber, M., Brändli, M., Bruno, G., et al. (2017). The Colour and Stereo Surface Imaging System (CaSSIS) for the ExoMars Trace Gas Orbiter. *Space Science Reviews*, 212, 1897–1944. <https://doi.org/10.1007/s11214-017-0421-1>
- Thomas, N., Hansen, C. J., Portyankina, G., & Russell, P. S. (2010). HiRISE observations of gas sublimation-driven activity in Mars' southern polar regions: II. Surficial deposits and their origins. *Icarus*, 205, 296–310. <https://doi.org/10.1016/j.icarus.2009.05.030>
- Thomas, P. C., Calvin, W., Cantor, B., Haberle, R., James, P. B., & Lee, S. W. (2016). Mass balance of Mars' residual south polar cap from CTX images and other data. *Icarus*, 268, 118–130. <https://doi.org/10.1016/j.icarus.2015.12.038>
- Thomas, P. C., Veverka, J., Lee, S., & Bloom, A. (1981). Classification of wind streaks on Mars. *Icarus*, 45, 124–153. [https://doi.org/10.1016/0019-1035\(81\)90010-5](https://doi.org/10.1016/0019-1035(81)90010-5)
- Titus, T. N., Kieffer, H. H., & Christensen, P. R. (2003). Exposed water ice discovered near the south pole of Mars. *Science*, 299, 1048–1051. <https://doi.org/10.1126/science.1080497>
- Toyota, T., Kurita, K., & Spiga, A. (2011). Distribution and time-variation of spire streaks at Pavonis Mons on Mars. *Planetary and Space Science*, 59, 672–682. <https://doi.org/10.1016/j.pss.2011.01.015>
- Valantinas, A., Thomas, N., Pommerol, A., Becerra, P., Hauber, E., Tornabene, L. L., et al. (2019). CaSSIS observations of fresh bright slope streak candidates in Arabia Terra. European Planetary Science Congress 13, abstract #1720-1.
- Valantinas, A., Thomas, N., Pommerol, A., Becerra, P., Hauber, E., Tornabene, L. L., et al. (2020). Multi-angular observations of Martian bright slope streaks. Lunar and Planetary Science Conference 51, abstract #2419.
- Verba, C. A., Geissler, P. E., Titus, T. N., & Waller, D. (2010). Observations from the High Resolution Imaging Science Experiment (HiRISE): Martian dust devils in Gusev and Russell craters. *Journal of Geophysical Research*, 115, E09002. <https://doi.org/10.1029/2009JE003498>
- Veverka, J., Thomas, P., & Greeley, R. (1977). A study of variable features on Mars during the Viking primary mission. *Journal of Geophysical Research*, 82, 4167–4188. <https://doi.org/10.1029/JS082i028p04167>
- Vincendon, M. (2015). Identification of Mars gully activity types associated with ice composition. *Journal of Geophysical Research: Planets*, 120, 1859–1879. <https://doi.org/10.1002/2015JE004909>
- Vincendon, M., Pílorget, C., Carter, J., & Stcherbinine, A. (2019). Observational evidence for a dry dust-wind origin of Mars seasonal dark flows. *Icarus*, 325, 115–127. <https://doi.org/10.1016/j.icarus.2019.02.024>
- Webster, C. R., Mahaffy, P. R., Atreya, S. K., Moores, J. E., Flesch, G. J., Malespin, C., et al. (2018). Background levels of methane in Mars' atmosphere show strong seasonal variations. *Science*, 360, 1093–1096. <https://doi.org/10.1126/science.aag0131>
- Wells, E. N., Veverka, J., & Thomas, P. (1984). Mars: Experimental study of albedo changes caused by dust fallout. *Icarus*, 58, 331–338. [https://doi.org/10.1016/0019-1035\(84\)90079-4](https://doi.org/10.1016/0019-1035(84)90079-4)
- Whelley, P. L., & Greeley, R. (2008). The distribution of dust devil activity on Mars. *Journal of Geophysical Research*, 113, E07002. <https://doi.org/10.1029/2007JE002966>
- Williams, K. E., Toon, O. B., & Heldmann, J. (2007). Modeling water ice lifetimes at recent Martian gully locations. *Geophysical Research Letters*, 34, L09204. <https://doi.org/10.1029/2007gl029507>
- Wilson, S. A., Howard, A. D., Moore, J. M., & Grant, J. A. (2016). A cold-wet middle-latitude environment on Mars during the Hesperian-Amazonian transition: Evidence from northern Arabia valleys and paleolakes. *Journal of Geophysical Research: Planets*, 121, 1667–1694. <https://doi.org/10.1002/2016JE005052>
- Wordsworth, R. (2016). The climate of early Mars. *Annual Review of Earth and Planetary Sciences*, 44, 381–408. <https://doi.org/10.1146/annurev-earth-060115-012355>
- Zimelman, J. R. (2019). The transition between sand ripples and megaripples on Mars. *Icarus*, 333, 127–129. <https://doi.org/10.1016/j.icarus.2019.05.017>